SAND78-0458
TTC-0087
Unlimited Release
Printed June 1981

Distribution
Category UC-71

ANALYSIS, SCALE MODELING, AND FULL-SCALE TEST OF A RAILCAR AND SPENT-NUCLEAR-FUEL SHIPPING CASK IN A HIGH-VELOCITY IMPACT AGAINST A RIGID BARRIER

Michael Huerta for
Applied Mechanics Division IV, 5524
Sandia National Laboratories
Albuquerque, NM 87185

ABSTRACT

This report describes the mathematical analysis, the physical scale modeling, and a full-scale crash test of a railcar spent-nuclear-fuel shipping system. The mathematical analysis utilized a lumped-parameter model to predict the structural response of the railcar and the shipping cask. The physical scale modeling analysis consisted of two crash tests that used 1/8-scale models to assess railcar and shipping cask damage. The full-scale crash test, conducted with retired railcar equipment, was carefully monitored with onboard instrumentation and high-speed photography. Results of the mathematical and scale modeling analyses are compared with the full-scale test.

DISCLAIMER

ACKNOWLEDGMENTS

Many Sandia personnel contributed to the work reported herein. H. R. Yoshimura (4552) was the project engineer in charge of the overall crash testing program. D. C. Bickel (1535) and R. L. Lucas (2323) designed the propulsion system and conducted the full-scale test. D. R. Stenberg, presently at Missouri Research Laboratories, assisted in preparing the hardware for the test and in taking measurements after the test. M. E. Barnett (1583) and W. V. Hereford (1582) were responsible for the instrumentation and telemetered data acquisition. T. A. Leighley (1556) was responsible for the high-speed film coverage. J. C. de Baca (1542) and W. W. Gravning (3153) obtained data from the high-speed films. J. Puhara (2453), R. Vantheemsche (2455), G. M. Haines (1485), and C. C. Bates (1247) drafted and constructed the scale models. T. G. Priddy (5522) and other personnel from the Engineering Analysis Department (5520) provided many valuable discussions on the engineering aspects of the project.

The author would like to thank the individuals mentioned above and others who have been of assistance to him in the course of this work and in the preparation of this document.

CONTENTS

ILLUSTRATIONS

ILLUSTRATIONS (continued)

ANALYSIS, SCALE MODELING, AND FULL-SCALE TEST OF A RAILCAR AND SPENT-NUCLEAR-FUEL SHIPPING CASK IN A HIGH-VELOCITY IMPACT AGAINST A RIGID BARRIER

Introduction

This report presents the analysis and results of a crash test of a railcar spent-nuclear-fuel shipping system. This test was conducted by Sandia Laboratories on September 27, 1977, for the United States Department of Energy. The railcar test is the third in a series to investigate various transportation systems for spent-nuclear-fuel shipping casks.[1] The first two tests provided data on the response of a truck-trailer system carrying spent-nuclear-fuel as it impacted a rigid barrier at high speed.[2] The railcar system impacted a concrete structure at a nominal velocity of 129 km/hr (80 mph). The system response was carefully monitored with high-speed photography and with onboard instrumentation operating through a telemetry package. One of the purposes of all these tests was to assess the engineering capability to predict the response of shipping systems to severe accidents while carrying spent-nuclear-fuel.

Before the full-scale tests were conducted, a thorough preliminary investigation was conducted to determine how the system would respond. Pretest analyses of the railcar test included mathematical lumped-parameter modeling and one-eighth scale-model tests, the results of which were given in an earlier report.[3] The present report describes the railcar system, the mathematical calculations, the scale-model tests, and the results of the full-scale test. A comparison of the results of the pretest analyses and the full-scale test is also presented.

The Railcar System

The railcar system used in the test was a retired unit built around 1960 (Figure 1). The railcar system consisted of a heavy steel frame with two three-axle trucks attached to cross bolsters on the frame, each truck weighing 9 metric tons (20,000 lbs). Part of the railcar system was the cask encasement structure (Figure 2), comprised of heavy steel components welded together and including a bolted down cover. The complete system, including the cask, weighed about 136 metric tons (300,000 lbs). The cask itself weighed 68 metric tons (150,000 lbs).

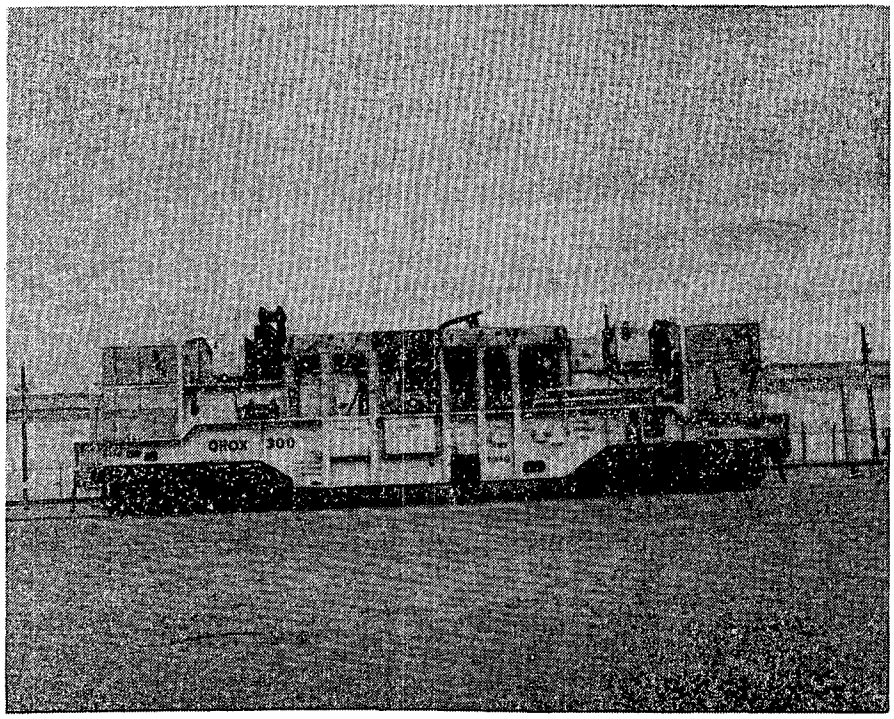

Figure 1. Railcar System as Acquired

Within the encasement structure, a cylindrical spacer (or filler) unit served to constrain any movement of the shipping cask (Figure 2). The wall of the cylinder was 1.27 cm (0.5 in.) thick. The cask and the spacer unit were clamped in place by inverted saddle structures on the bolted down cover. Four half-inch-thick gusset plates at each end of the encasement structure axially restrained the cask and spacer unit, and acted as a bumper system for the encasement structure.

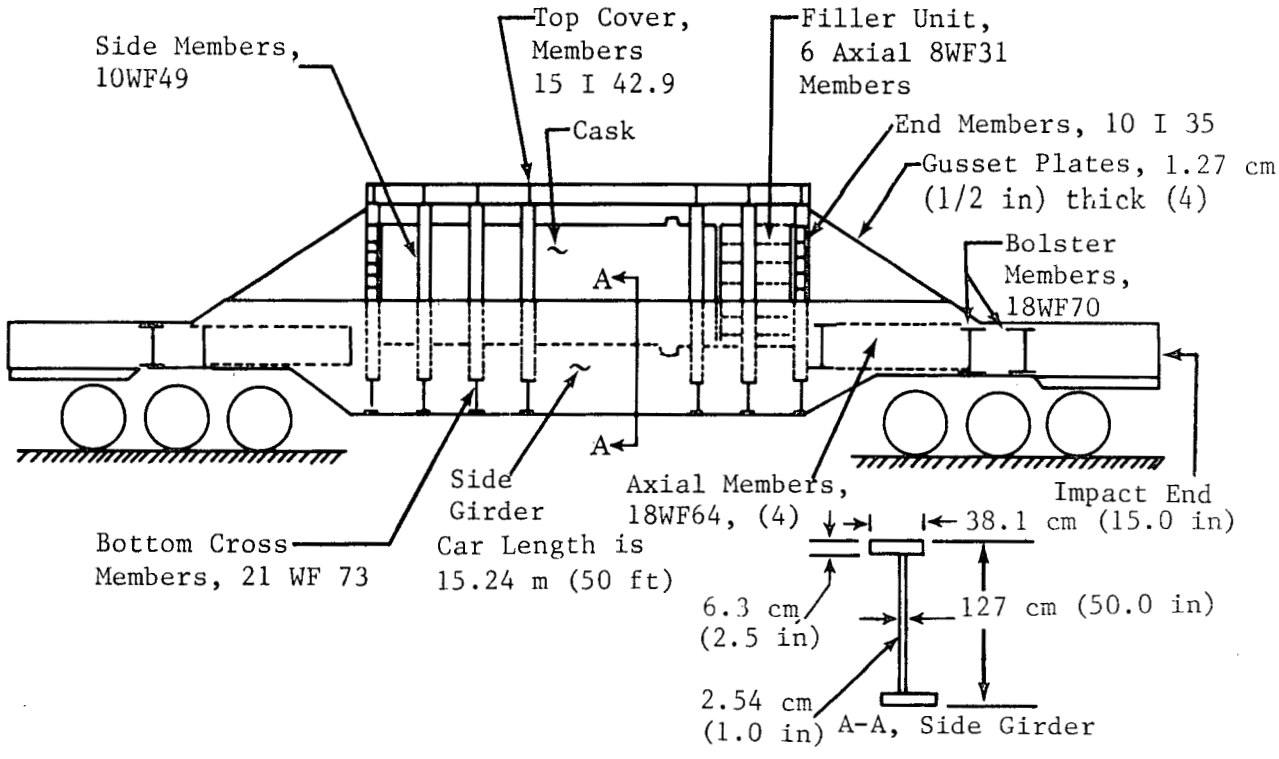

Figure 2. Schematic of the Railcar Structure

The shipping cask was made of stainless steel with lead shielding (Figure 3). The outer shell was 3.5 cm (1.375 in.) thick and the inner shell was 0.95 cm (0.375 in.) thick. The outer diameter of the cask was 157 cm (62 in.) and its overall length was 394 cm (153 in.). The cask head contained heavy stainless steel plates, lead shielding, and a pump cavity. It was attached to the cask body with twenty-four 3.2-cm (1-1/2-in.) high-strength bolts. The fuel cavity, with space for 10 fuel assemblies, was normally water-filled when transporting fuel.

In the test, the cask carried nine mock assemblies and one real, but unirradiated, unit. Figure 4 is a photograph of the fuel rod assembly (depleted uranium) carried in the water-filled cask.

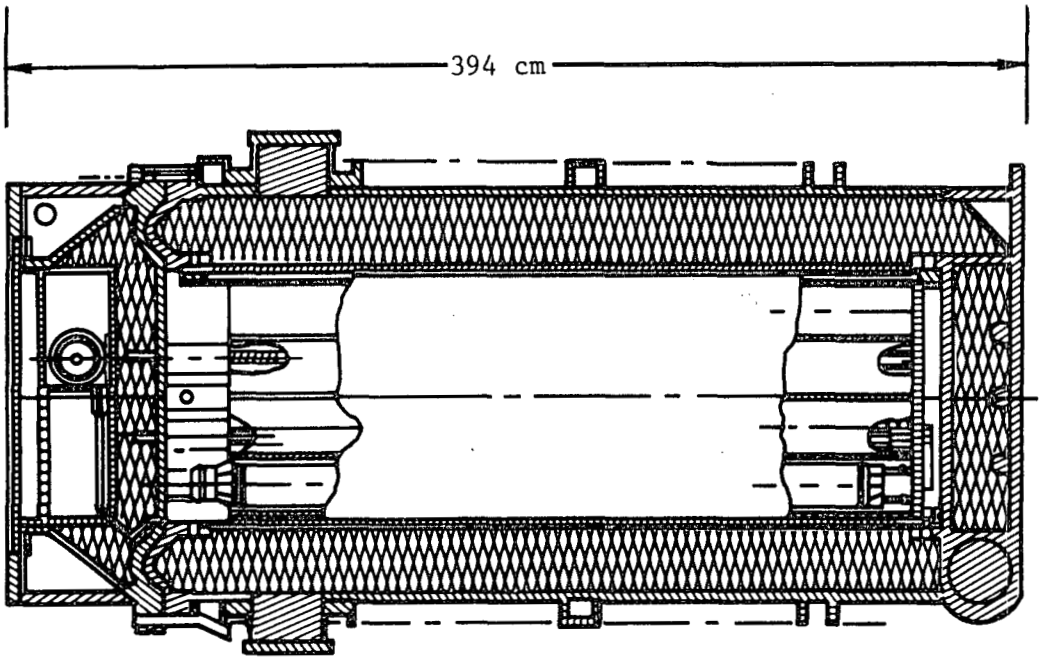

Figure 3. Schematic of the Shipping Cask

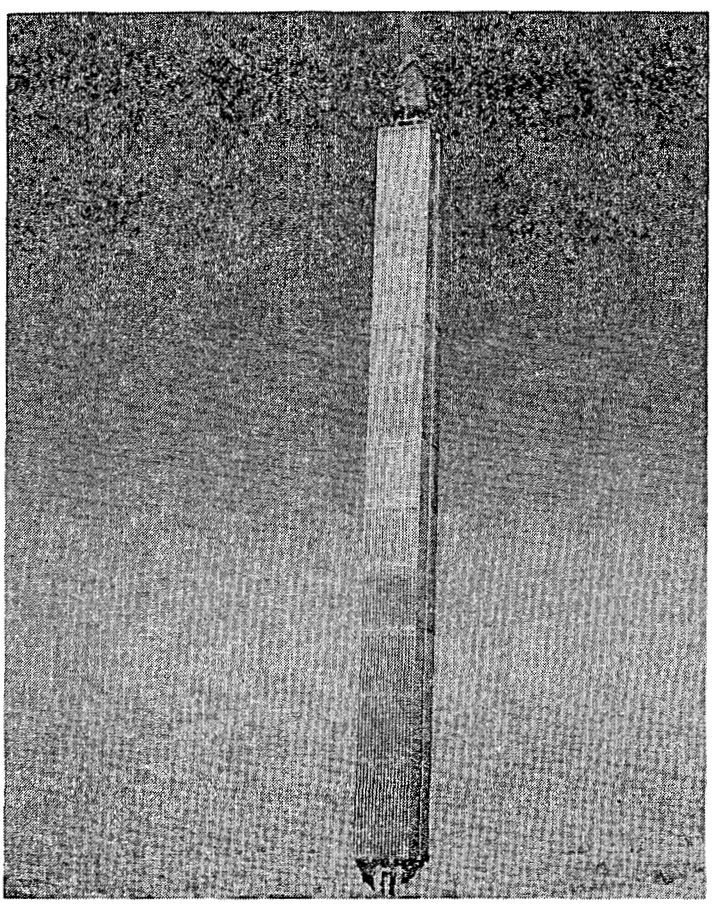

Figure 4. Fuel Rod Assembly

Mathematical Analysis

Methodology

Preliminary calculations based on the crush strength of the railcar structure, the center of gravity, and the rotational inertia of the system indicated that there would be no appreciable rotation of the railcar structure upon impact. Hence, the problem, judged to be essentially one-dimensional, was analyzed by using a one-dimensional lumped-parameter model. In this type of model, the system is discretized into mass elements and coupling (spring) elements. The model is then used in conjunction with a computer program to calculate the dynamic response of the system. Figure 5 is a schematic of the lumped-parameter model formulated to analyze this problem.

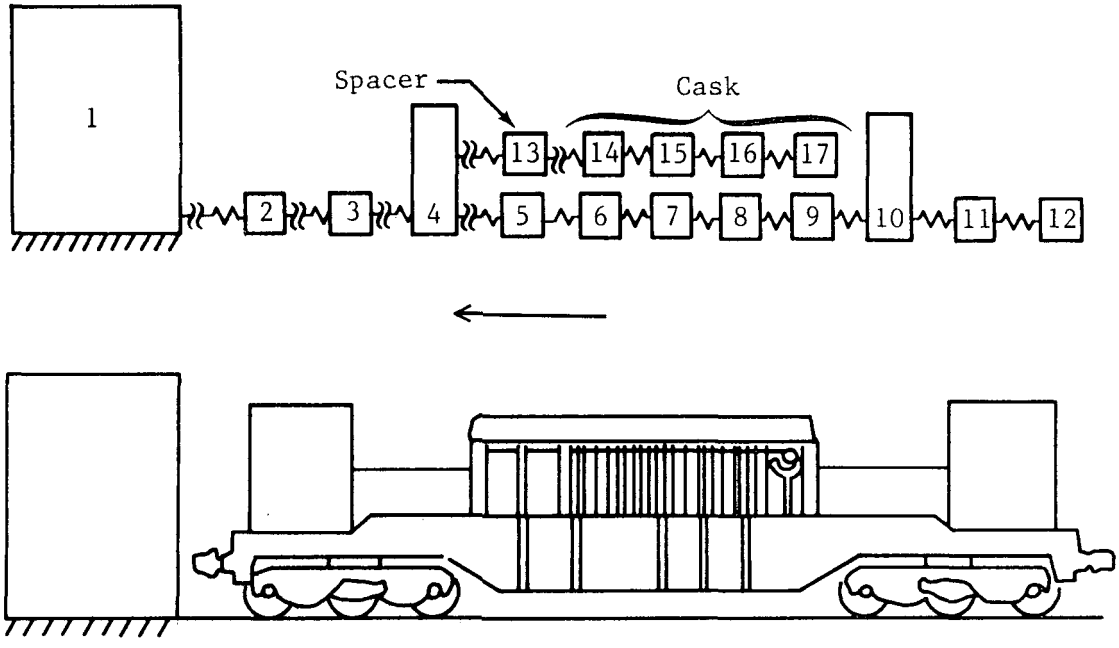

Figure 5. Schematic of the Lumped Parameter Model

The railcar structure in Figure 5 is represented by mass elements 2 through 12. Mass 13 represents the spacer unit and mass elements 14 through 17 represent the cask. Mass 1, the target, was assumed to be fixed. The coupling elements for the model were derived from structural analysis estimates of the force-displacement characteristics for each

element of the structure. The impact was simulated by giving all the mass elements, except the target, an initial velocity equal to the projected full-scale impact velocity of the test. The SHOCK[4] computer program was used with this model to calculate the dynamic response of the system (see Appendix A for details).

Results

For an impact at 129 km/hr (80 mph), calculations indicated that the front end of the railcar structure would crush about 250 cm (100 in.). Calculations also indicated that the cask would move essentially as a rigid body within the encasement structure, partially crushing the spacer unit. Forces acting on the cask were not calculated to be great enough to plastically deform its basic structure. Only deformations to external cooling fins and small imprints on the head area were believed to be possible.

Figures 6 and 7 reflect some results of calculations made with this model. Figure 6 shows the cask displacement as a function of time, with zero being the time of contact between the front end of the system and the target. It was calculated that the cask would displace forward about 300 cm (120 in.) in 0.145 s. Figure 7 illustrates the calculated cask velocity as a function of time. The calculations indicated that the cask would decelerate very uniformly, reaching a zero horizontal velocity in about 0.145 s. The railcar structure would stop even more quickly with the cask continuing to move forward within the encasement structure. The maximum rigid-body deceleration levels for the cask were calculated to be about 30 g.

Thus, the lumped-parameter model showed that a 129 km/hr (80 mph) impact would not cause permanent deformations to the cask. However, such an impact would crush the front end of the railcar structure, causing the cask to move forward within the encasement structure, partially crushing the spacer unit. The mathematical analysis was verified by the results of scale-model tests--the next step in the analysis.

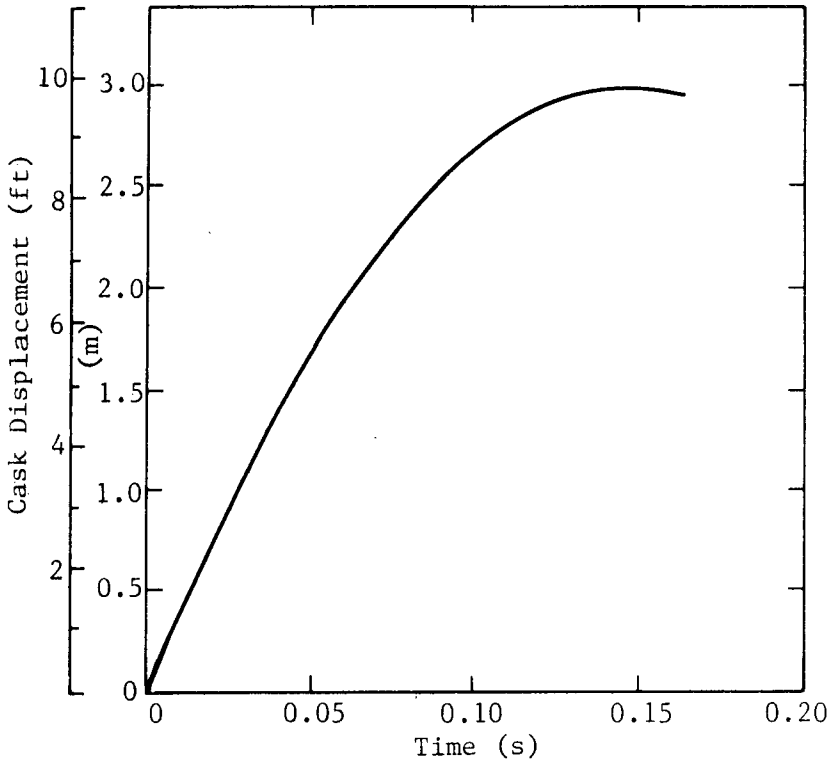

Figure 6. Cask Displacement as a Function of Time, Computed With the Lumped-Parameter Model

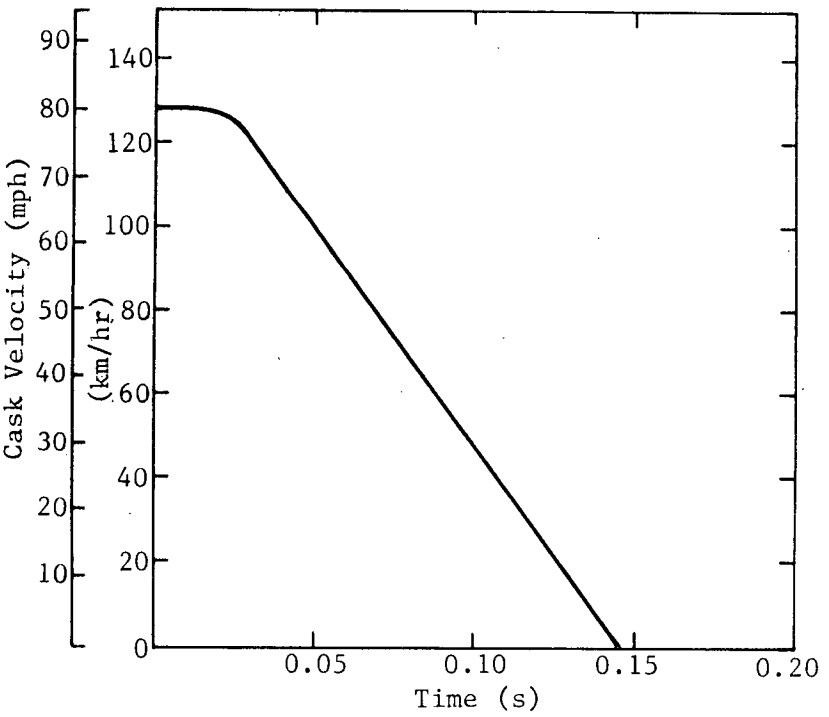

Figure 7. Cask Velocity as a Function of Time, Computed With the Lumped-Parameter Model

Scale Models

The scale models were designed to predict the behavior of the full-scale system. Only the pertinent structural features were included in the models, similar to the modeling technique used in the tractor-trailer crash test.[2] In the report describing that test, a more complete discussion of scale modeling is presented. A description of the scale models constructed for the railcar study and the results of scale-model impact tests will be presented here. The results will be shown to confirm the mathematical analysis.

The models used in this study consisted of the railcar structure, the cask, and the filler unit. Because the railcar was the most significant structure in terms of system response, more planning went into the design and construction of this model than into that of the cask model. Construction details of the system model are included in Appendix B. Figure 8 is a schematic of the complete one-eighth scale model. The materials were similar to those in the prototype.

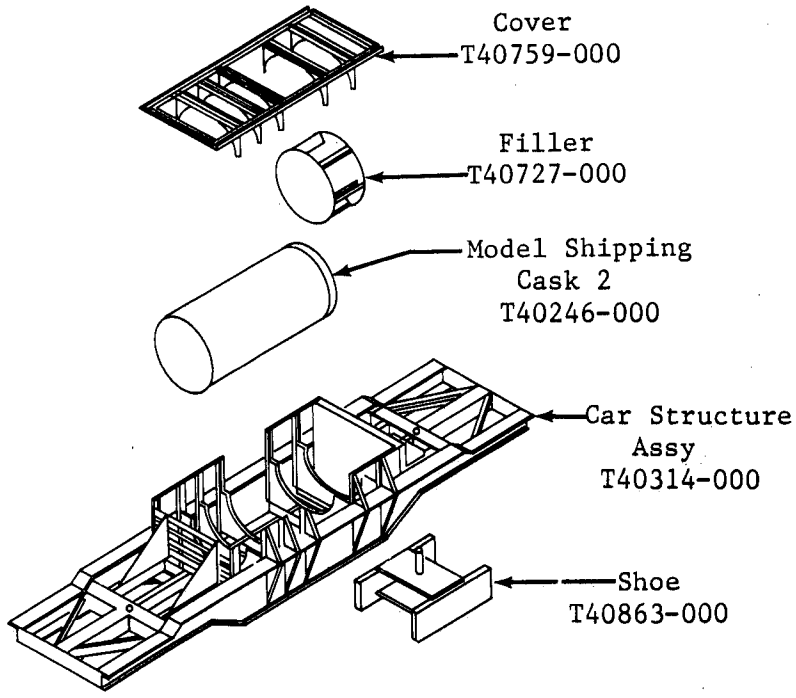

Figure 8. Schematic of the One-Eighth Scale Model

The railcar was constructed of small stock-sections and plates welded into place (Figure 9). The model shipping cask consisted of concentric steel tubing with welded end-plates. The railcar cover, which clamps the cask and the spacer unit in place, was bolted to the railcar structure with scaled-down bolts. The model was designed to run on a sled track and the shoes on the model simulated the railcar trucks.

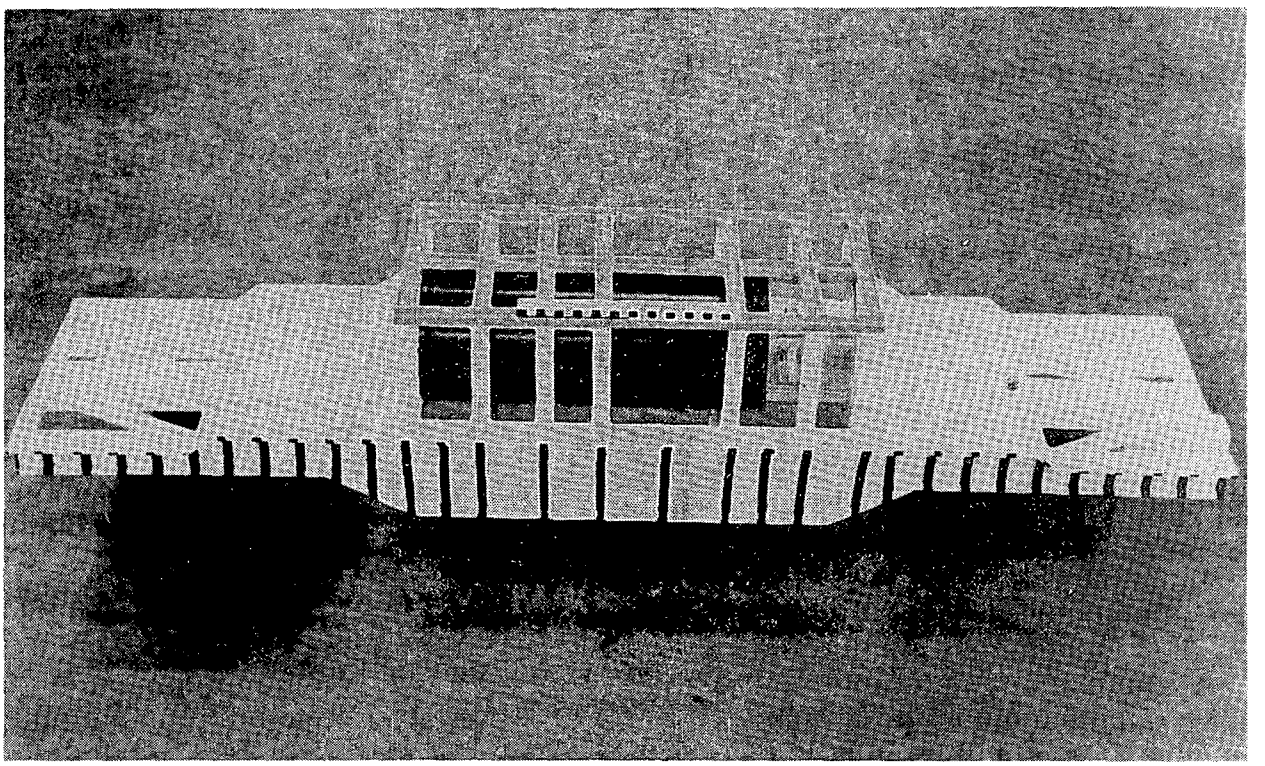

Figure 9. Photograph of the Scale Model

Two scale-model tests were conducted at nominal impact velocities of 129 km/hr (80 mph). In the first test, the railcar impacted against a concrete target. In the second test, it impacted against a more massive steel-faced concrete block. Figures 10 and 11 illustrate the sequence of events observed in the first test, against the concrete target.

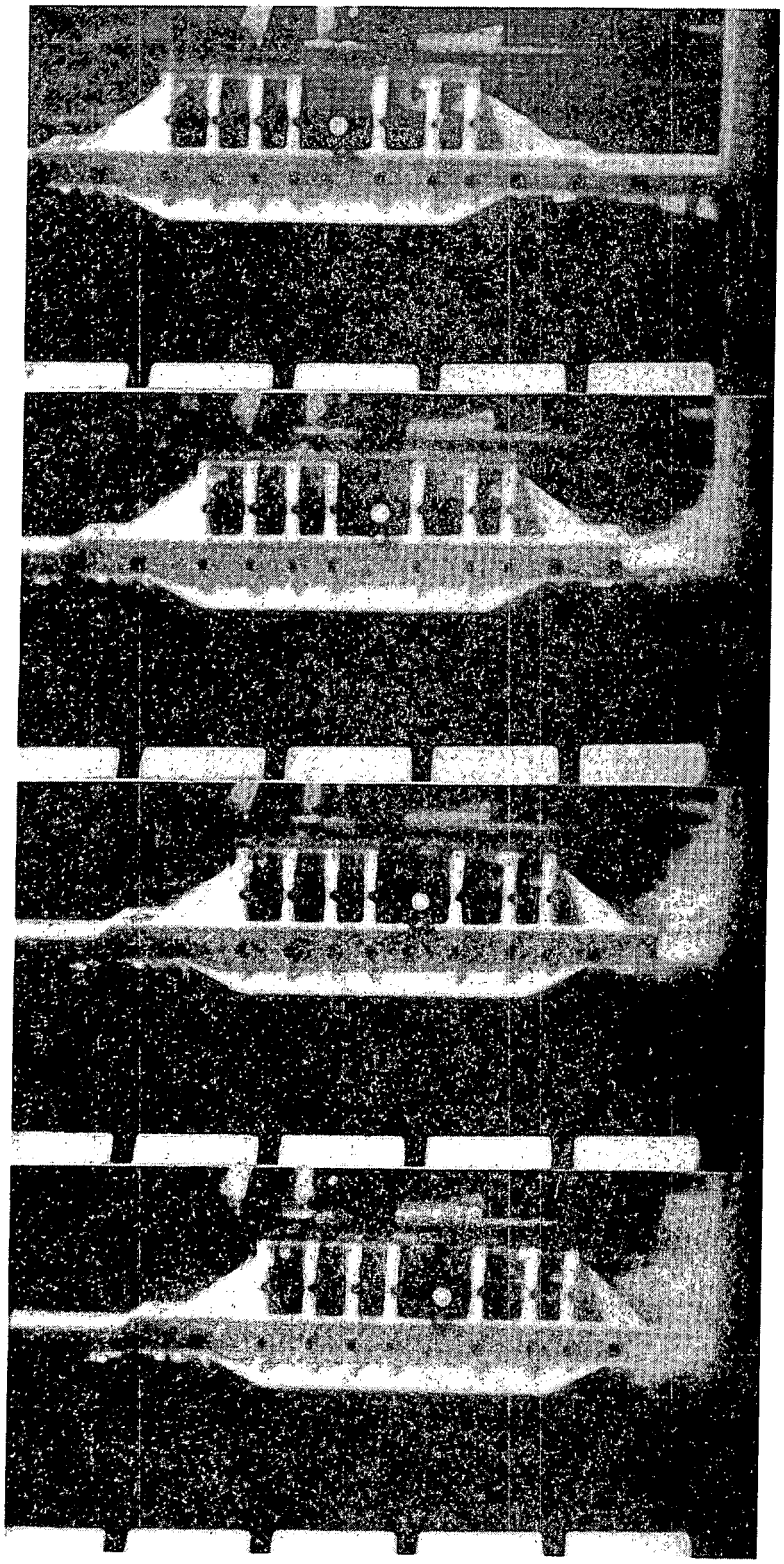

Figure 10. Early Sequence of Events in the First Scale-Model Test

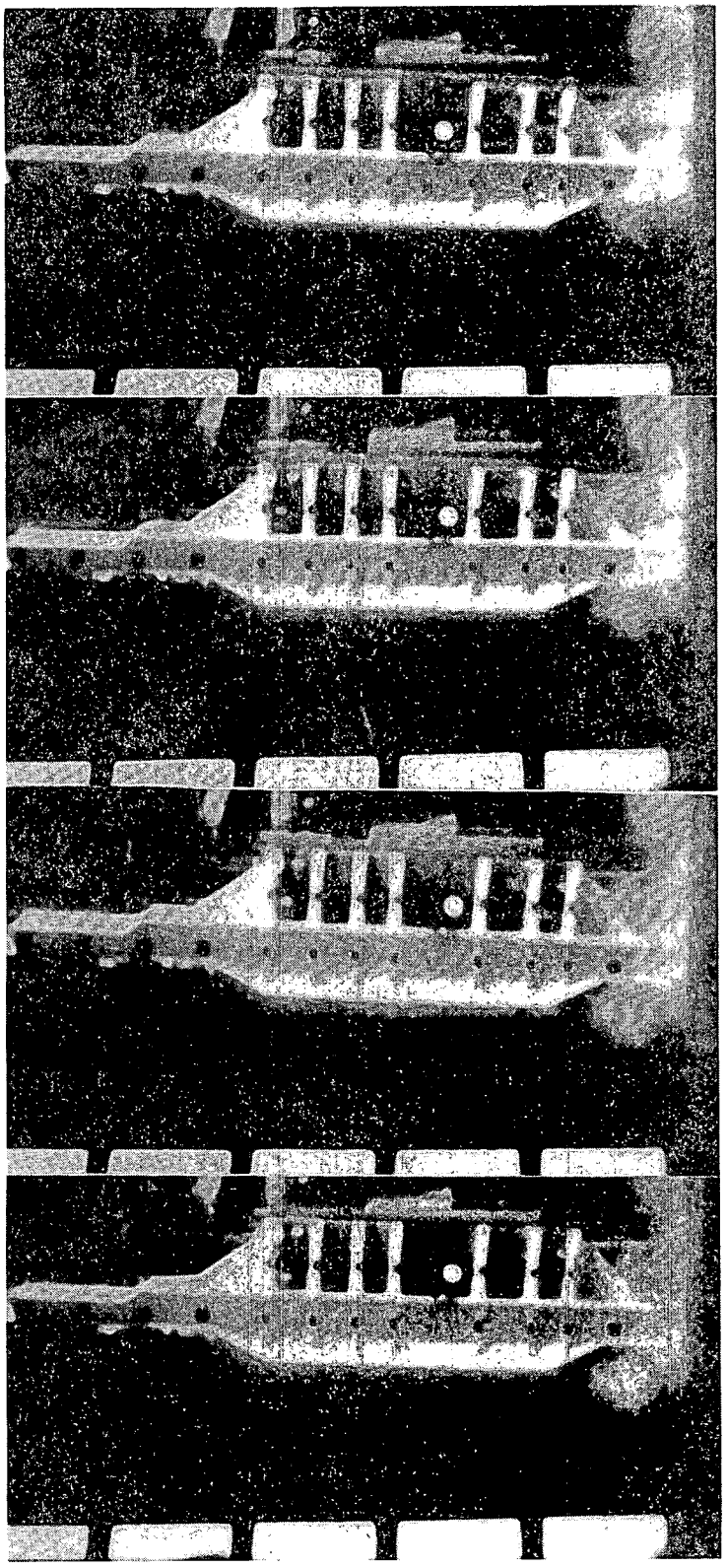

Figure 11. Late Sequence of Events in the First Scale-Model Test

The model response in the first test was consistent with what had been predicted by the mathematical analysis (Appendix C contains data from both of the scale model tests). The system remained nearly horizontal as the front end of the structure crushed; then, towards the end of the impact, the system began rotating, with the back end rising. The crash of the railcar crushed back the front end of the structure ~20 cm (8 in.), almost to the front bolster. The cask moved forward within the encasement structure, partially crushing the spacer unit, yet remaining virtually undamaged. The bumper system on the railcar structure yielded slightly, deflecting more at the top. The railcar encasement cover was nearly detached from the structure; most of the retaining screws were broken, but remained in place. Photometric analysis of the films indicated that the cask decelerated fairly uniformly through the impact and came to a horizontal stop in 0.020 s. This model response indicated that the full-scale cask impact would take 0.160 s, since events in the scale-model tests occur more quickly by the scale factor than in the prototype. (With a one-eighth scale model, the scale factor is 8.)

The second test, in which the railcar impacted the steel-faced target, yielded basically the same results; however, the front end of the railcar structure and the spacer unit underwent a slightly greater deformation. Also, the railcar cover was completely dislodged in this test. Despite these effects, the cask remained undamaged as in the first test. Figures 12 and 13 illustrate the sequence of events in the second test.

The difference in impact behavior observed in the two tests was attributed primarily to the deflection of the concrete target in the first test. Upon impact, the concrete target deflected somewhat because the backing soil was not firm enough to support it. In the second test, the supporting soil was well tamped. In addition, the concrete target in the second test was faced with a 5.1-cm (2-in.)-thick steel plate. The second test was an attempt to model the worst possible case. It was expected that the full-scale system response would fall somewhere between the two responses observed in the scale-model tests. Both scale-model tests indicated that the cask would come through the impact virtually undamaged, despite the extensive damage to the front end of the railcar.

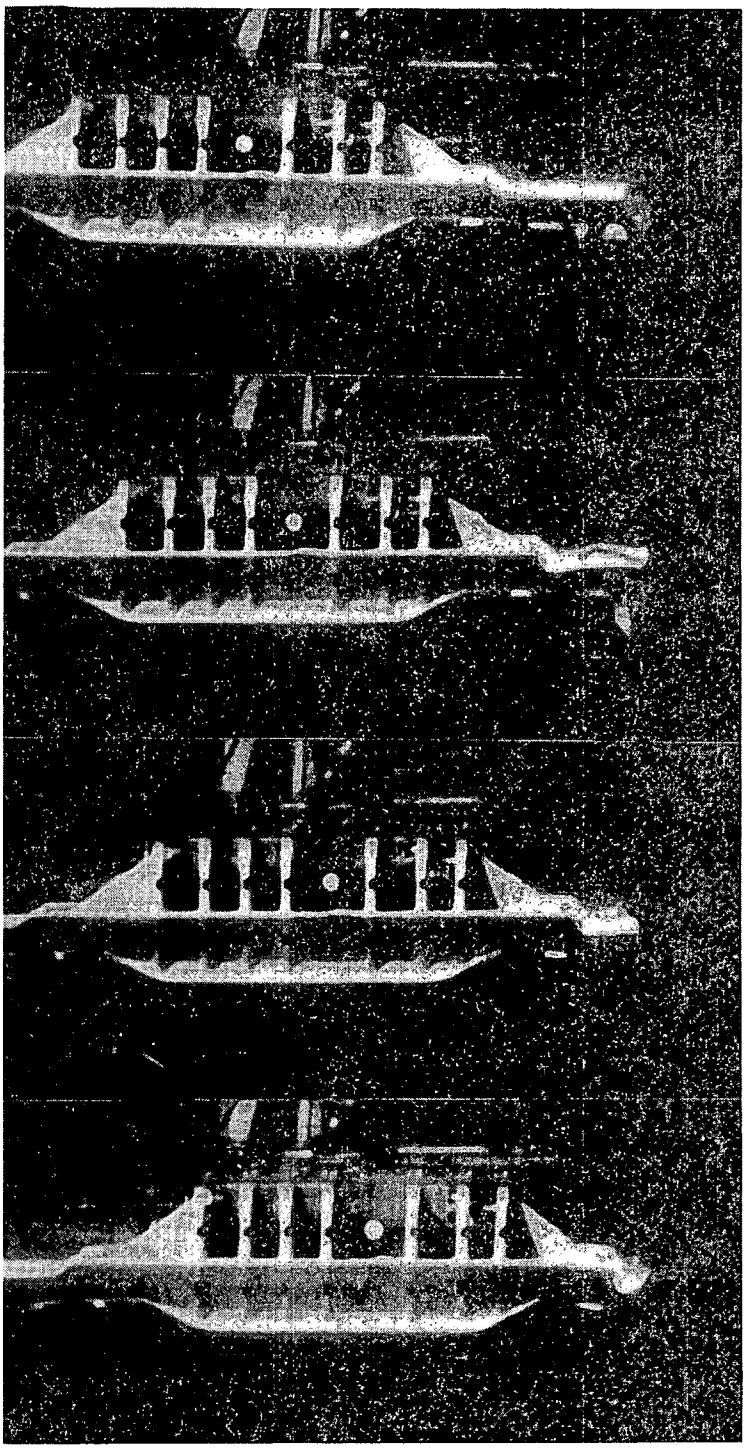

Figure 12. Early Sequence of Events in the Second Scale-Model Test

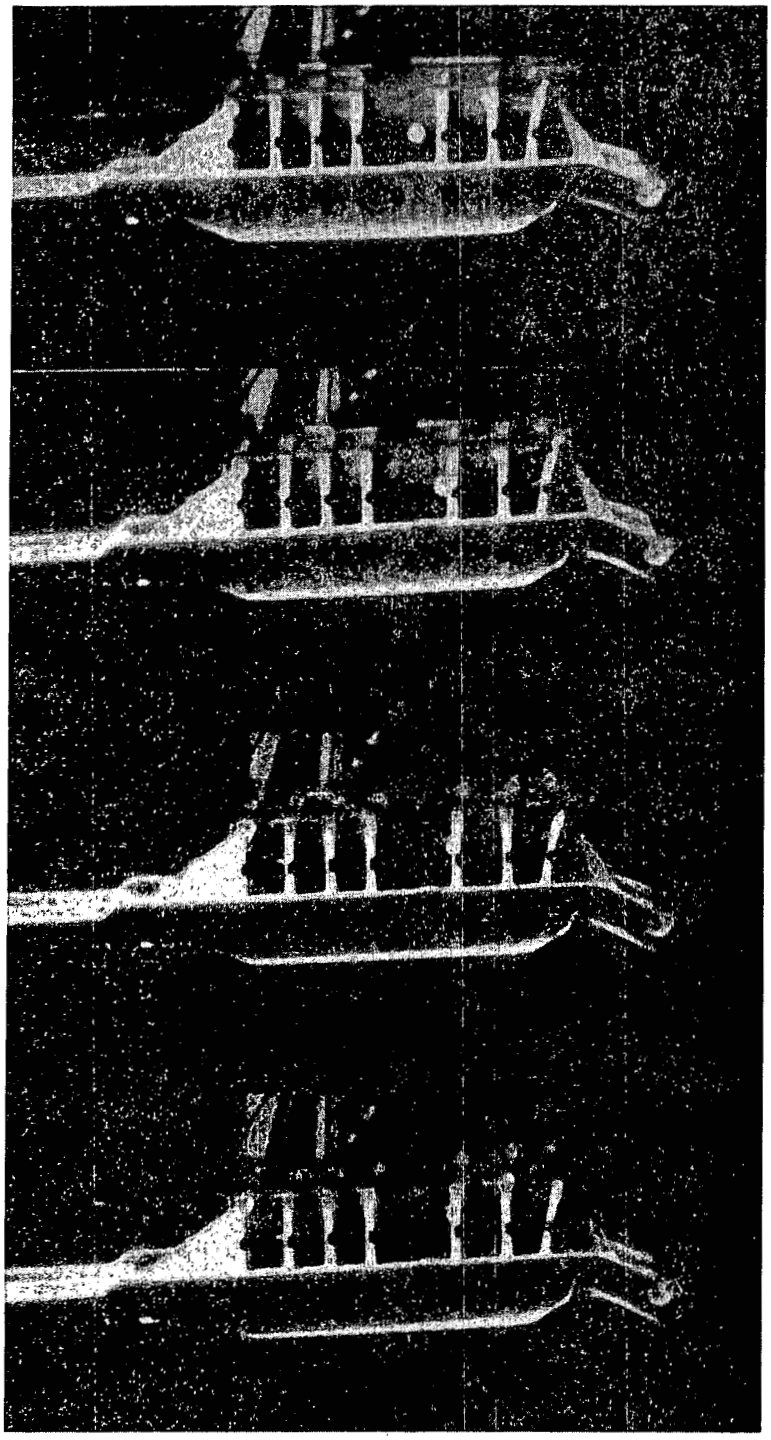

Figure 13. Late Sequence of Events in the Second Scale-Model Test

Full-Scale Test

Test Description and Hardware

The full-scale test was conducted at a sled track facility where the system was accelerated to speed and allowed to coast into a specially constructed, rigidly reinforced concrete target. The system was propelled by a cluster of 24 rocket motors attached to a pusher sled. A water brake separated the pusher from the railcar at a point near the target, allowing the railcar system to coast into the target.

The hardware for the test was carefully prepared in terms of pretest inspection and instrumentation. Bright-colored paint on the hardware made it more visible in the photocoverage. Figure 14 shows the cask being lowered into the railcar structure. Figure 15 illustrates the assembled system with the pusher sled. Three onboard cameras were installed on the back end of the car to film the event. The cameras as well as the system of rocket motors are more clearly visible in Figure 16, which shows the back end of the system. Figure 17 is a close-up view of the concrete target, which was also used for the tractor-trailer crash tests.[2] A long-range view of the track (Figure 18) shows the guiderails and overhead cameras. A more complete description of the target structure is given in the tractor-trailer crash test report.[2]

Instrumentation

Extensive high-speed film coverage, with filming rates up to 3000 frames/second, was provided for the test. Ground cameras on both sides of the track and overhead cameras in front of the track were aimed at the impact side from various angles. Data from the photography coverage were gathered and digitized.

The active telemetered instrumentation onboard the railcar included on-off switches, strain gages, and piezoresistive accelerometers. Strain gages were installed on the front end of the railcar frame, on the cask head and body, and on two fuel rods inside the cask. Accelerometers were placed on the railcar, railcar cover, and on the cask. Either "crush" or

"breakwire" on-off switches were used to indicate when the system contacted the target, when the cask began to move relative to the railcar, and when the trucks sheared from the frame. Some accelerometers were also placed near the top of the target surface. Two telemetry packs on the railcar transmitted the signals from the onboard instrumentation. These data were recorded on magnetic tape, then digitized and plotted.

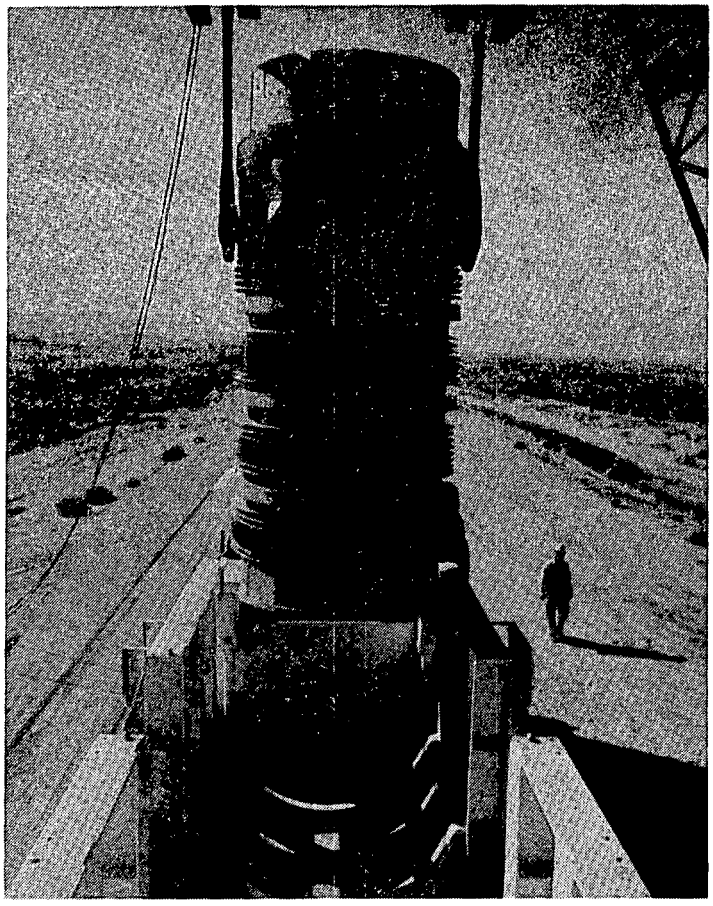

Figure 14. Full-Scale Cask Being Lowered Into the Railcar

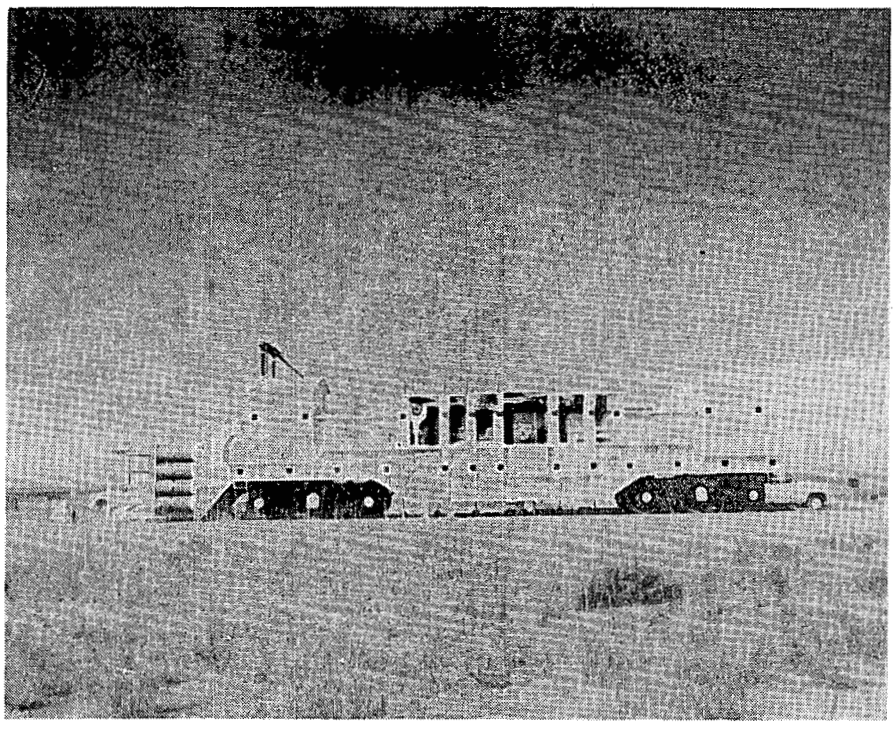

Figure 15. The Full-Scale System Assembled

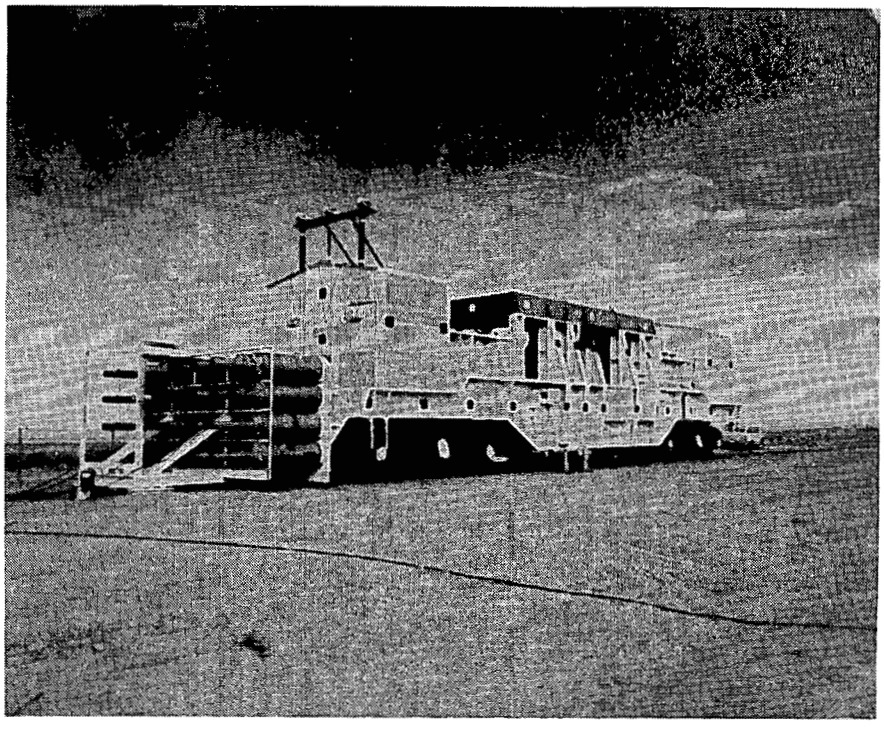

Figure 16. Back End of the System Including the Rocket Motors

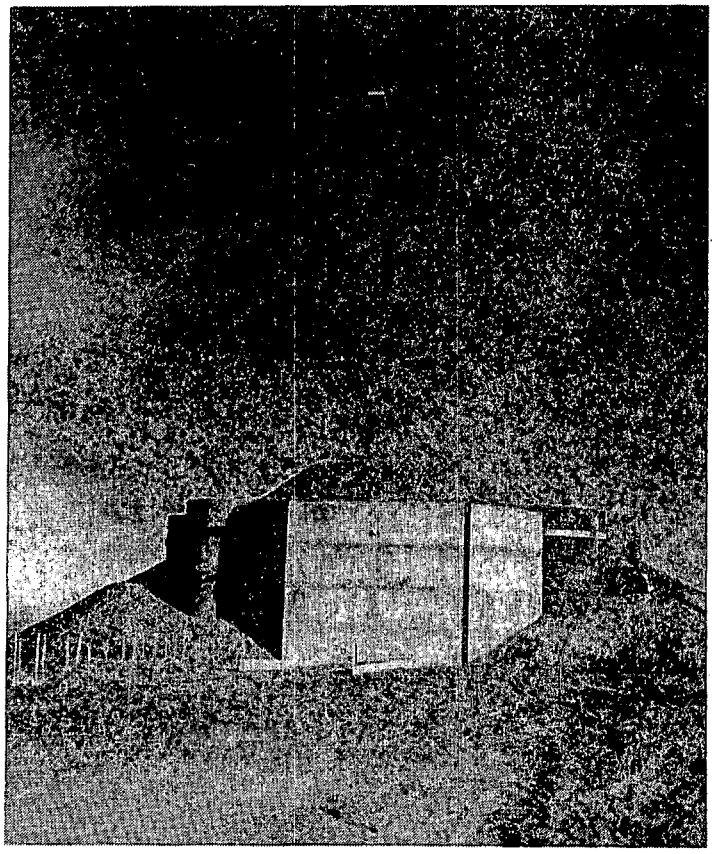

Figure 17. Close-Up View of the Concrete Target

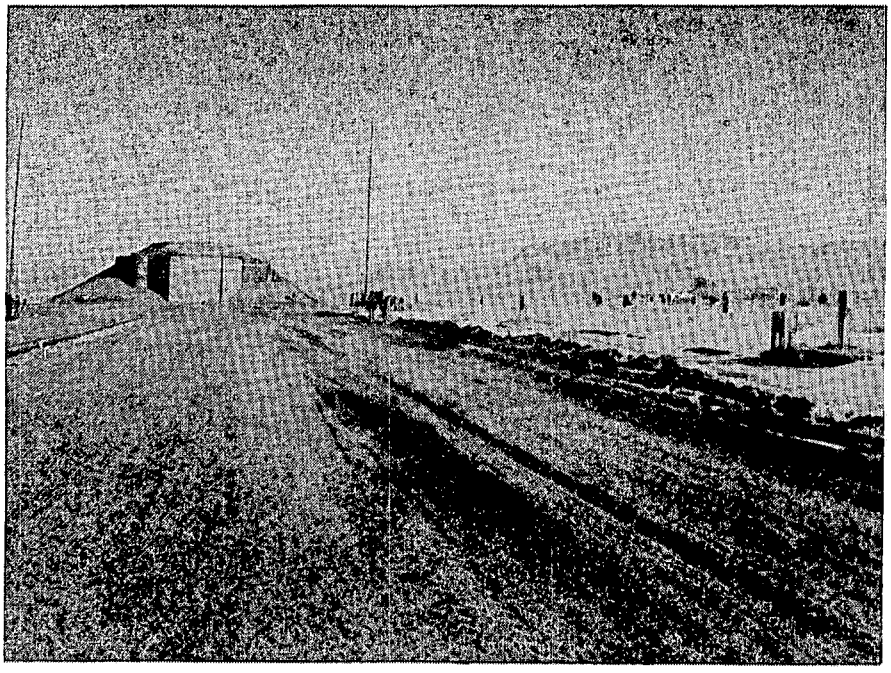

Figure 18. Long-Range View of the Concrete Target Including the Guiderails and Overhead Cameras

Results

The full-scale system was successfully launched and impacted at a velocity of 131 km/hr (81 mph). Figures 19, 20, and 21 illustrate the sequence of events during the first 250 ms of the impact, with time zero being the instant the coupler contacted the wall. The impact resulted in extensive damage to the railcar structure, but damage to the target was minimal; the target deflection was negligible. The two trucks simultaneously sheared from the frame at about 25 ms, the rear trucks scooting forward under the frame and coming to rest near the front of the vehicle. The vehicle structure itself came to a horizontal stop in ~140 ms while the cask continued to move forward within the railcar structure for another 50 ms. The front end of the railcar was crushed back nearly to the front bolster, and the resultant forward movement of the cask completely crushed the spacer unit* (Figures 22, 23 and 24). The railcar cover remained in place with the saddle structures failing in a hinge mode. The cask body itself was completely undeformed except for minor deformations to external cooling fins (Figure 25). There was no leakage. Subsequent examination of the fuel rods, contained within the cask, revealed that they were undamaged. Only the support bracket at the end of the bundle was slightly distorted (Figure 26).

The photography coverage and the onboard instrumentation functioned quite well, although a number of telemetry signals were lost before the end of impact. Analysis of the films provided displacement-time data that were used to generate a deceleration-time curve for the cask. A point near the center of the cask was followed to analyze the cask motion (Figure 27). The film data indicated that the cask underwent a deceleration value of about 32 g. Additional film data is included in Appendix D.

---

*The spacer unit crushed completely due to the fact that the axial I beams indicated in drawings were left out of the unit during its construction. Because the unit was a sealed cylinder, the absence of the I-beams was not noticed in the examination of the hardware. This discrepancy caused some error in the analyses and allowed the cask to travel further than anticipated.

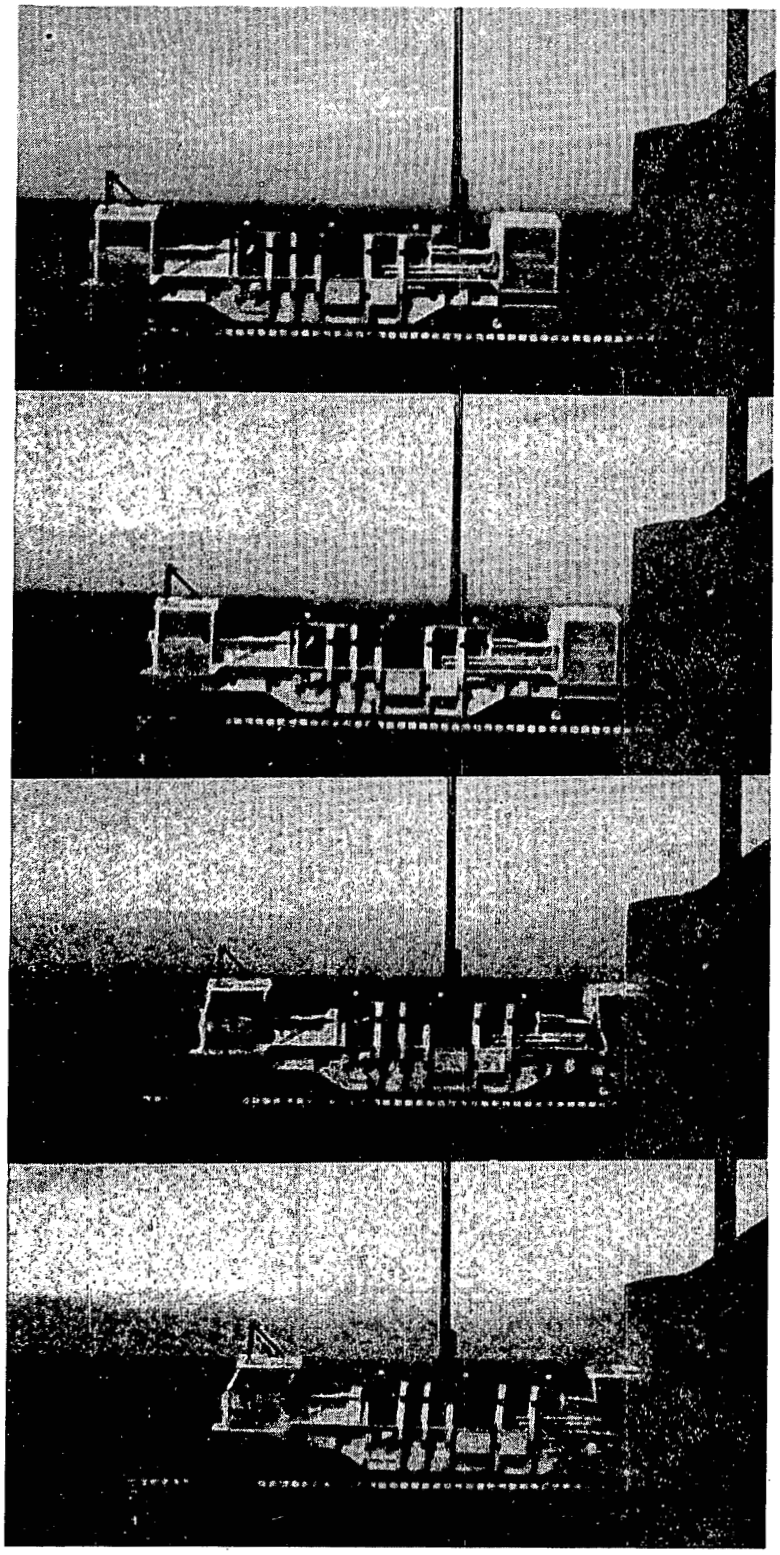

Figure 19. Full-Scale Test Sequence of Events From -0.025 to 0.050 s

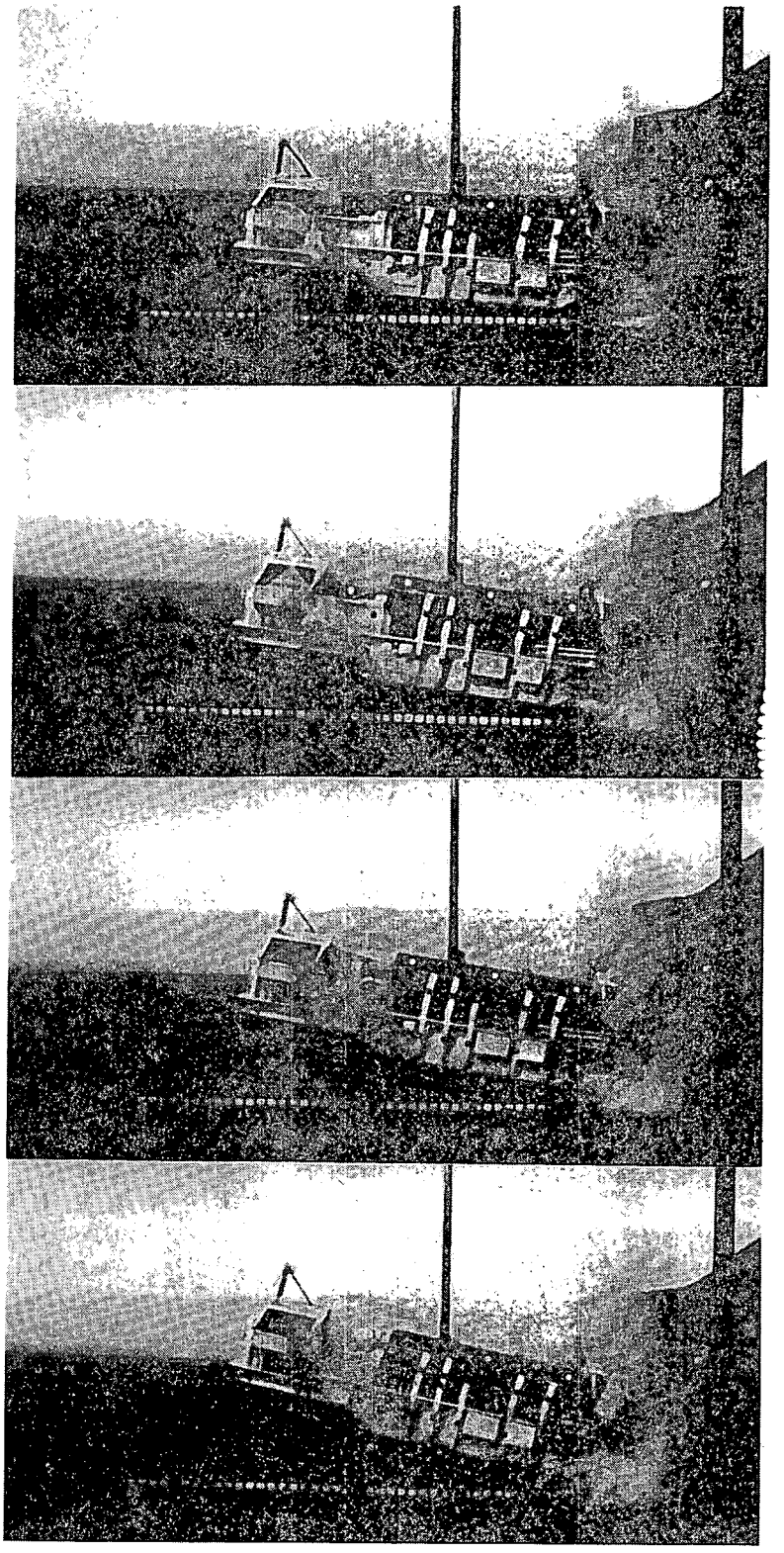

Figure 20. Full-Scale Test Sequence of Events From 0.075 to 0.150 s

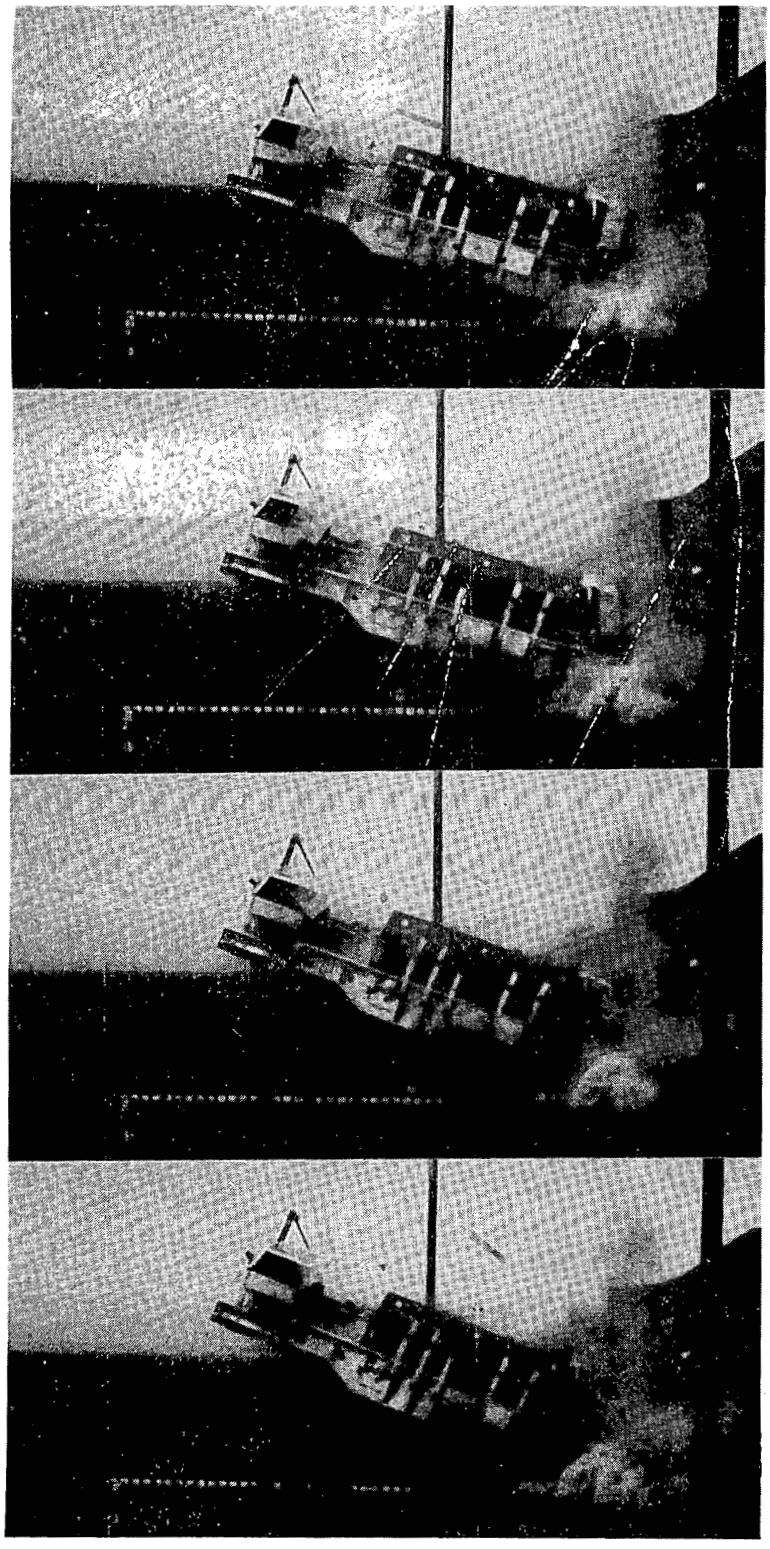

Figure 21. Full-Scale Test Sequence of Events From 0.175 to 0.250 s

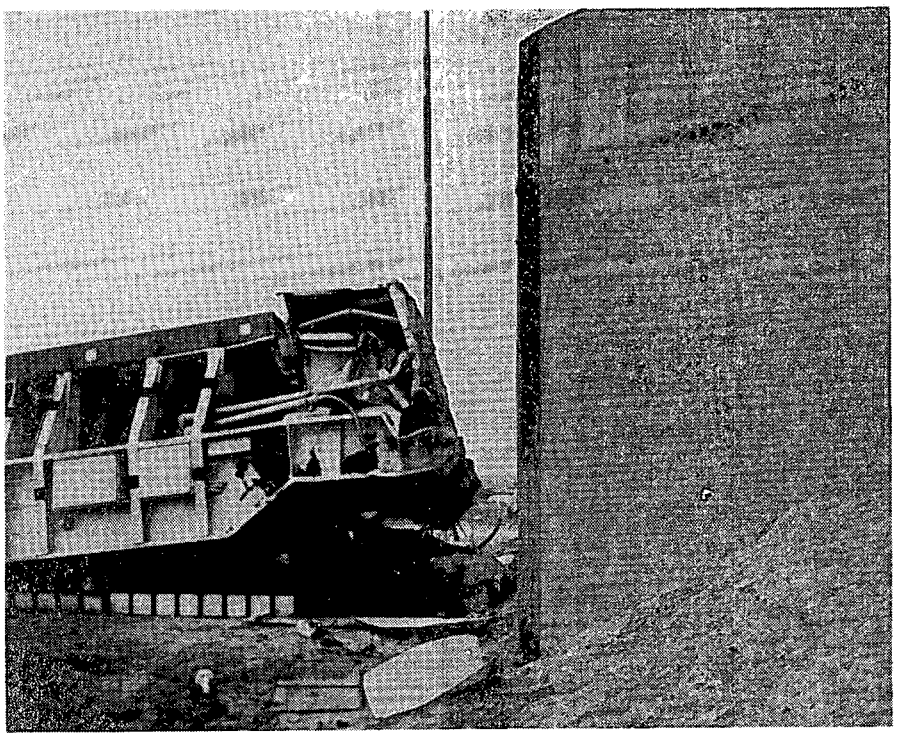

Figure 22

Front End of the Full-Scale System After Impact

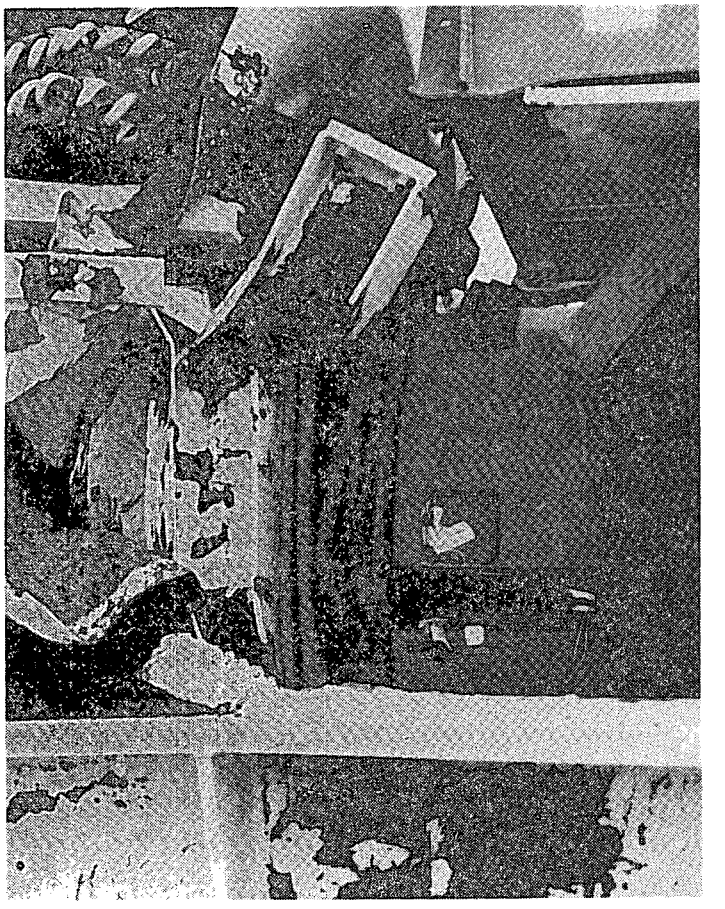

Figure 23.

Close-Up View of the Front End of the Cask and the Spacer Unit After Impact

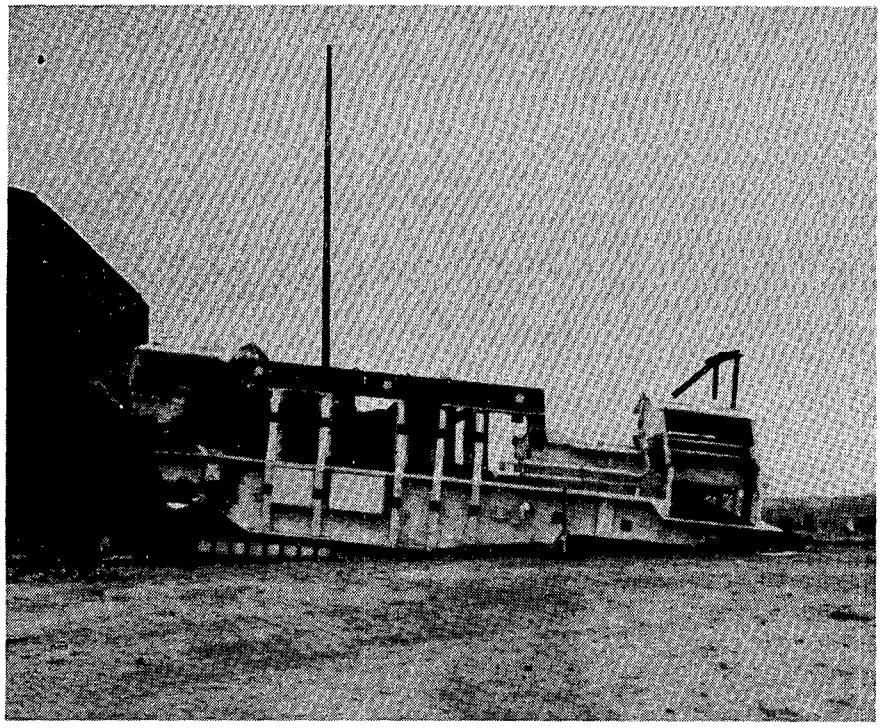

Figure 24. Side View of the Full-Scale System After Impact

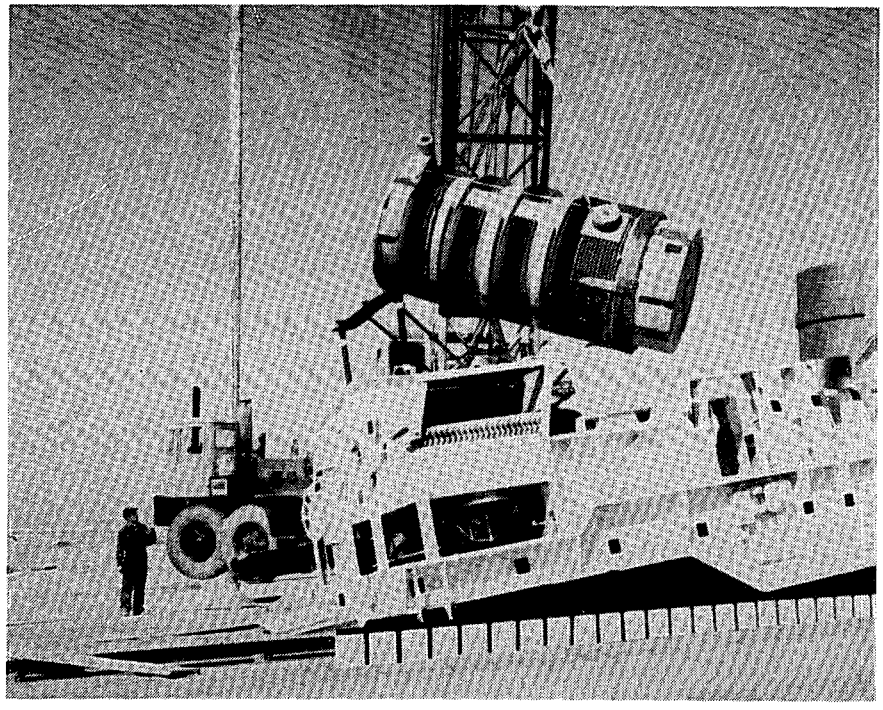

Figure 25. Shipping Cask After Impact

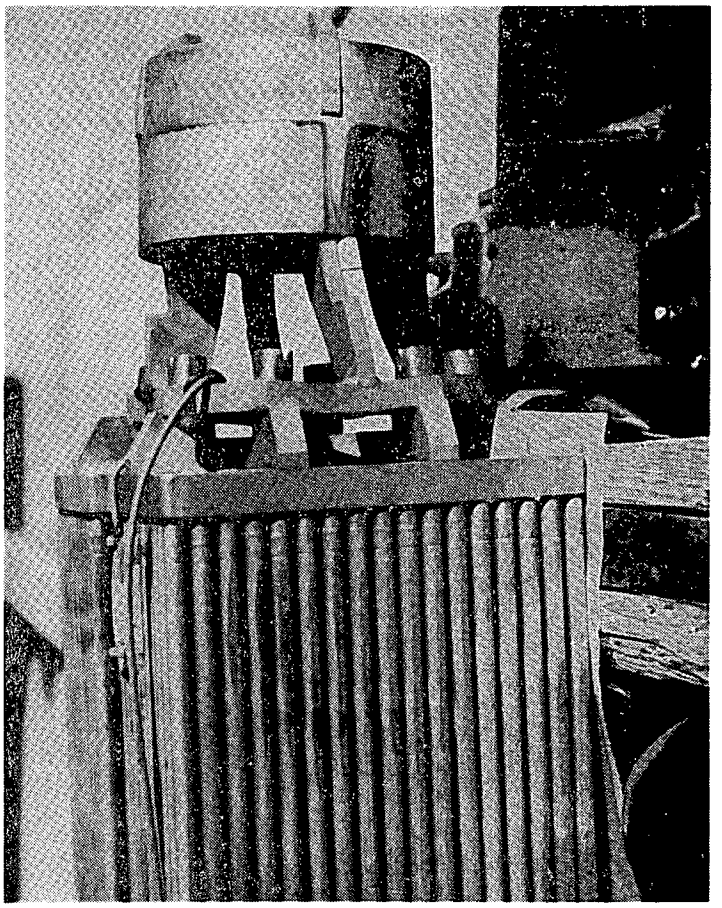

Figure 26.

Impact End of the Fuel Bundle

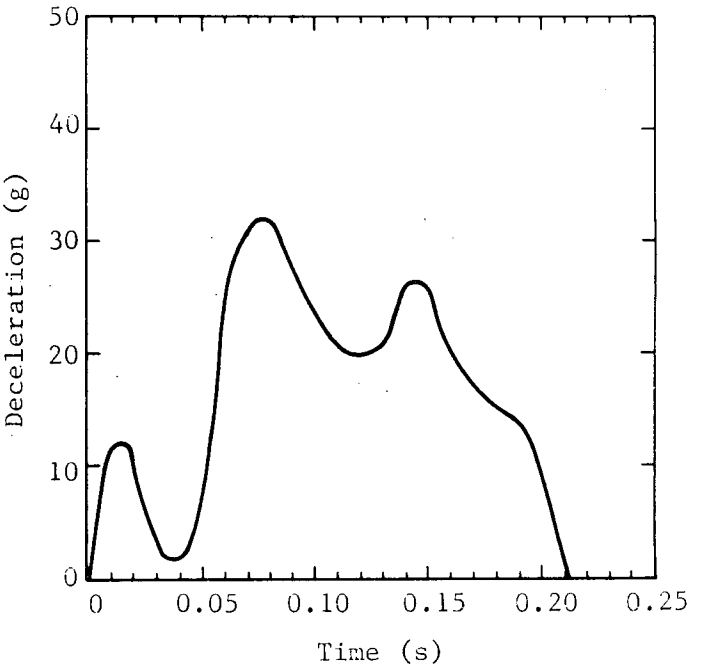

Figure 27.

Cask Deceleration vs Time (film data)

Only one complete deceleration plot for the cask was obtained from the onboard instrumentation. This data, included in Appendix D, indicated a peak value somewhat higher than that obtained from film data. Appendix D also contains a plot of deceleration vs time for a point on the railcar structure near the front. The deceleration recorded on the railcar with the accelerometers was considerably higher than that recorded on the cask. The railcar accelerometers recorded peak readings above 100 g. Film data, analyzed by following a point near the back of the structure, indicated a peak value of about 40 g.

The strain gage readings from the front of the railcar frame (approximately above the center of the trucks) indicated that the strains at this point went plastic at about 20 ms. Readings from the strain gages on the right side of the cask were higher than those on the left, indicating impact at a slight angle. In addition, the strains on the head were higher than those on the cask body. However, all cask strains were within the elastic limit, indicating that the cask was not permanently deformed. The strains recorded for the fuel rods (see appendix D) were also within the elastic limit.

Discussion

Deceleration plots obtained from film data have been found to yield peak values that were lower than values obtained from onboard instrumentation data. This was found to be the case in the truck-trailer study as well, yet the reasons for this are not completely clear. It is believed that the film data values are more realistic figures to use because integration of the film acceleration-time curve produces the correct velocity change for the impact. The accelerometer data, although filtered, is probably still somewhat biased by high frequencies. The film data is considered to be more representative of what can be termed a rigid body motion of the cask.

To evaluate the recorded strains, the yield point of the stainless steel cask and fuel rod cladding can be taken to be about 1100 x 10^{-6} cm/cm. The fuel rod gages, aligned along the principal stress direction, can produce a direct comparison to this value using the data in Appendix D. The data indicate that peak stresses in the fuel rods reached a point that was about 50% of the yield value. The highest recorded stresses were on the right side of the cask head. The stress at this point reached about 75% of the yield but the stress on the left side appeared to reach a value of only 25% of the yield. Therefore, the average stress in the cask head reached an apparent average value of 50% of the yield point. Stresses on the cask body were considerably lower. These numbers are rough approximations and are presented merely to show the estimated severity of the stresses induced in the cask and fuel rods.

Comparison of Analysis and Scale Model Tests to Results of Full-Scale Test

The full-scale test generally correlated well with the predicted results. The mathematical analysis predicted that the front end of the railcar would crush significantly and that the cask would move slightly forward within the encasement structure. It also predicted that the cask would come to a horizontal stop in approximately 0.145 s and that it would not be deformed in the impact. These results were generally verified by both the scale-model and full-scale tests, although the missing spacer I-beams in the full-scale system did introduce some error.

The full-scale test results also agreed well with the analyses in a kinematic sense. The system crushed without rotating significantly. The time duration of the impact, the displacement of the cask, and the velocity-time history of the cask occurred almost as predicted by the mathematical analysis and the scale-model tests. Figures 28 and 29 compare the results quantitatively. Figure 28 illustrates the displacement of the cask as a function of time. As can be seen, the displacement was somewhat underestimated, primarily because the spacer unit crushed a great deal more than expected. It was later discovered that the spacer unit had

not been equipped with the internal I-beams (Figure 2). Another reason for the discrepancy in displacement-time for the full-scale test was that the railcar system yielded slightly more than expected (Figure 23).

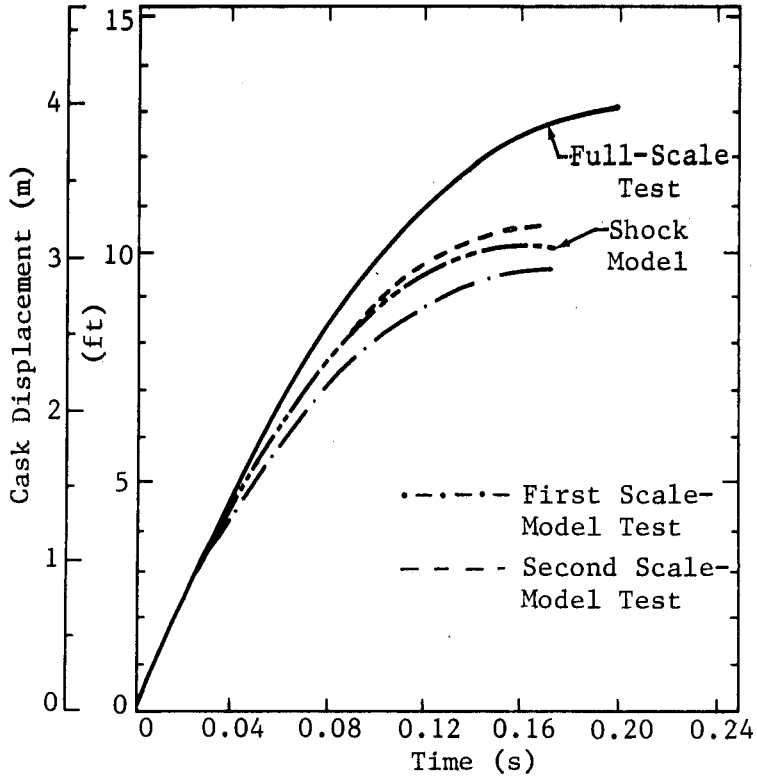

Figure 28. Cask Displacement as a Function of Time (film data)

Figure 29, the velocity-time history for the cask from the analysis, scale-model tests, and full-scale test, illustrates the considerable agreement among the three curves. However, the full-scale system decelerated more slowly due to greater cask displacement. This greater cask displacement was mainly due to the large amount of crush sustained by the spacer unit. Also, the full-scale system appears to have had quite a bit of slack which was not included in the model. Another possible explanation for the variations between the analyses and test is that in the film analysis, the initial point of impact could have been taken somewhat early in time. Nevertheless, despite these discrepancies, the correlations are still considered good.

The analytical and scale-model analyses predicted that the body of the cask would not be stressed past its elastic limit and that components in front of the cask would crush before the cask would be damaged. This crush-up did indeed happen in the full-scale test. If the spacer unit had contained axial I-beams, it is believed that the cask still would have been undamaged since it was calculated that the cask head and body could take considerably more axial load than the spacer before yielding. Use of the I-beams in the full-scale test would have resulted in less cask displacement and better agreement with the analyses.

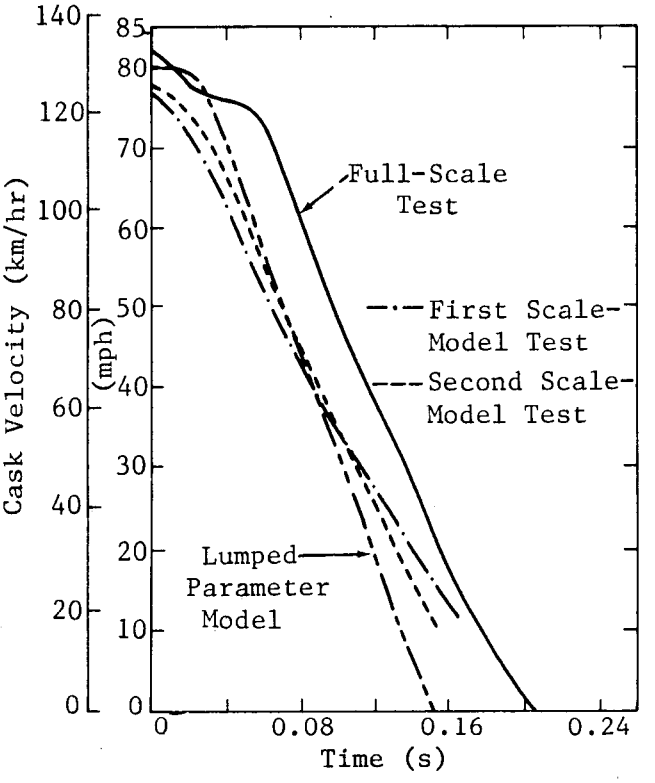

Figure 29. Cask Velocity as a Function of Time (film data)

The railcar structure itself responded close to pretest predictions. The front end of the car crushed approximately as expected. The mathematical analysis predicted ~2.5 m (100 in.) of crush and the full-scale system crushed back ~2.0 m (80 in.). The damage to the front end of the railcar was also similar to that observed in the scale-model tests. However, the bumper system deflected a little more than was expected. Thus, the analyses modeled the front end of the car on the "soft" side and the bumper system on the stiff side.

The bolting system designed for the railcar cover on the scale model was less sturdy than the one on the full-scale vehicle, causing the model cover to dislodge in the second model test. The bolting system was weak because the scale model lacked partially concealed shear pins that were included in the full-scale system. Yet, even the cover dislodgement in the second model test did not influence the response of the cask. Agreement, therefore, between the predicted and observed responses of the railcar structure is still considered good.

Conclusion

Both the mathematical analysis and the scale-model tests were able to predict, with a reasonable degree of accuracy, the response of a complex rail spent-nuclear-fuel-shipping system involved in an extremely severe accident. These techniques have also been successfully demonstrated in the analysis of a highway system.[2] This study further validates the techniques and demonstrates an engineering capability of predicting the response of spent-nuclear-fuel shipping casks and associated transport structures involved in severe impacts.

The same basic techniques along with good engineering judgment can be used to evaluate new transportation system designs and different environments which accident-probability studies indicate should be investigated. These techniques will provide more accurate results when applied to equipment that is better defined and with fewer structural uncertainties. This equipment would also have the benefit of newer technology and more stringent quality control measures than the older, retired systems. This will make possible the construction of more precise analytical and scale models. This study, along with the work in Reference 2, has demonstrated that indeed it is possible, with present analytical tools, to predict the response of spent-nuclear-fuel transportation systems involved in extremely severe impact situations.

APPENDIX A

Details of the Lumped Parameter Model

APPENDIX A

Details of the Lumped Parameter Model

The lumped parameter model (Figure 5) was used in conjunction with the SHOCK computer program.[4] Given some initial conditions, SHOCK numerically solves the second-order differential equations of motion associated with a spring-mass model. Spring (coupling) definitions may be nonlinear and can load and unload along different paths, simulating a hysteresis effect.

The model in this study made extensive use of the HYSTER option in the SHOCK program to simulate crush-up of structures. The HYSTER couplings are illustrated in Figures A.1. The mass and linear spring values used are listed below. The first mass was held fixed, therefore its value is irrelevant. The coupling definitions were structural analysis estimates based on measurements made of the hardware and expected yield strength values of the materials.

M_2	= 11,793 kg (26,00 lbm)	M_{10}	= 2,948 (6,500 lbm)
M_3	= 11,339 kg (25,000 lbm)	M_{11}	= 11,793 (26,000 lbm)
M_4	= 2,948 kg (6,500 lbm)	M_{12}	= 7,484 (16,500 lbm)
M_5	= 2,267 kg (5,000 lbm)	M_{13}	= 1,814 (4,000 lbm)
M_6	= 2,721 kg (6,000 lbm)	M_{14}	= 17,009 (37,500 lbm)
M_7	= 2,494 kg (5,500 lbm)	M_{15}	= 17,009 (37,500 lbm)
M_8	= 2,041 kg (4,500 lbm)	M_{16}	= 17,009 (37,500 lbm)
M_9	= 1,814 kg (4,000 lbm)	M_{17}	= 17,009 (37,500 lbm)
K5-6	= 3.50×10^8N/cm (2.0×10^8lb/in.)	K10-11	= 2.85×10^8N/cm (1.63×10^8lb/in.)
K6-7	= 2.71×10^8N/cm (1.55×10^8lb/in.)	K11-12	= 2.08×10^8N/cm (1.19×10^8lb/in.)
K7-8	= 5.44×10^8N/cm (3.11×10^8lb/in.)	K14-15	= 3.94×10^8N/cm (2.25×10^8lb/in.)
K8-9	= 5.44×10^8N/cm (3.11×10^8lb/in.)	K15-16	= 3.94×10^8N/cm (2.25×10^8lb/in.)
K9-10	= 4.20×10^8N/cm (2.40×10^8lb/in.)	K16-17	= 3.94×10^8N/cm (2.25×10^8lb/in.)

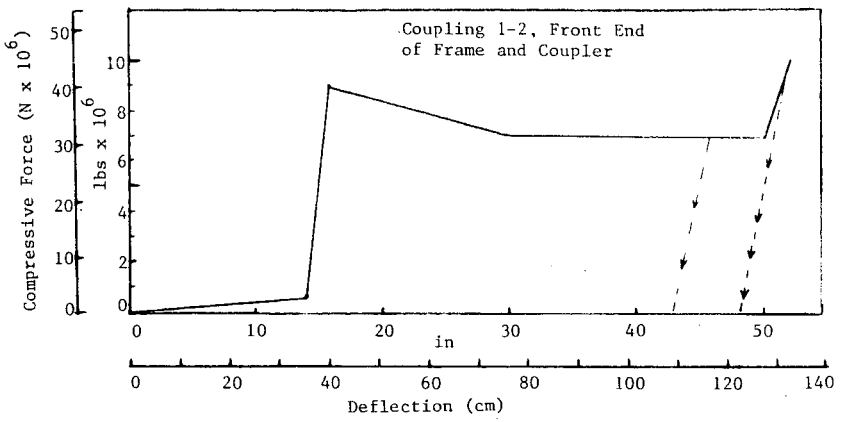

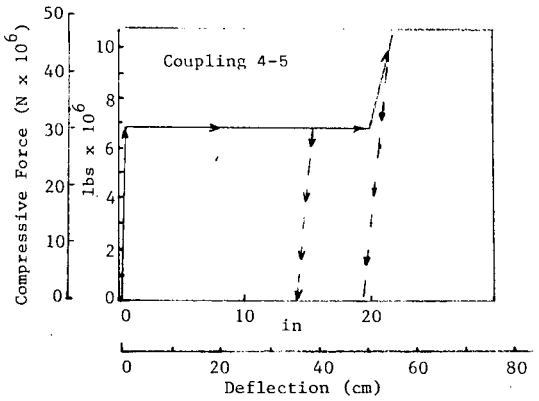

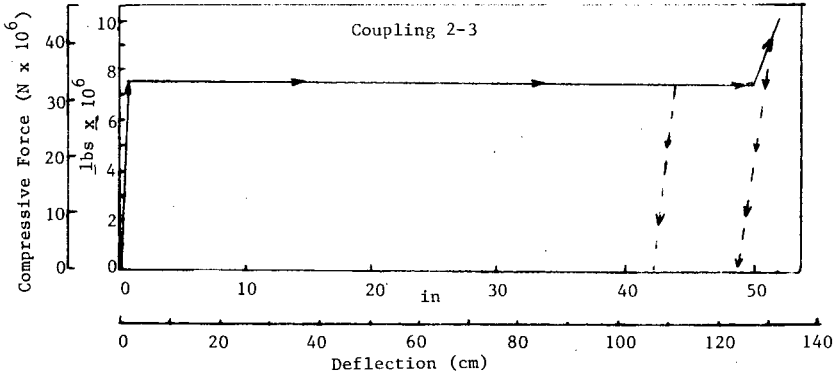

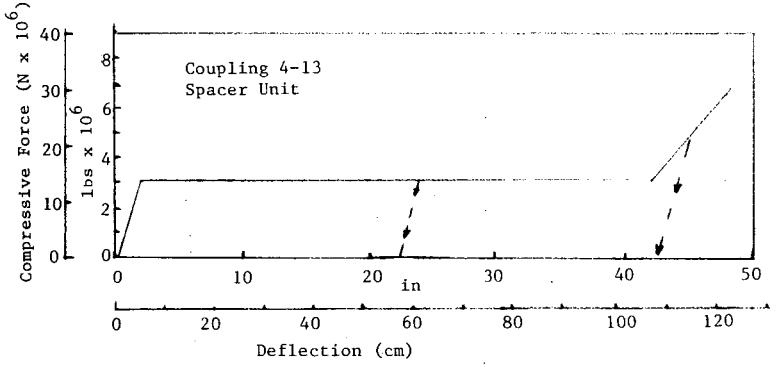

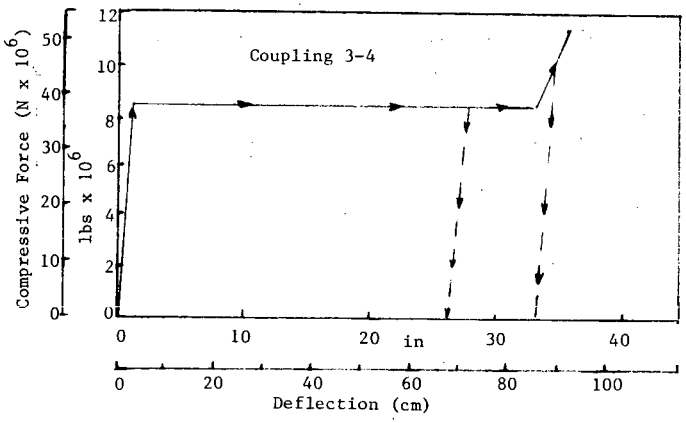

Figure A.1 Hysteresis Coupling Definitions

APPENDIX B

Construction Details for the Scale Models

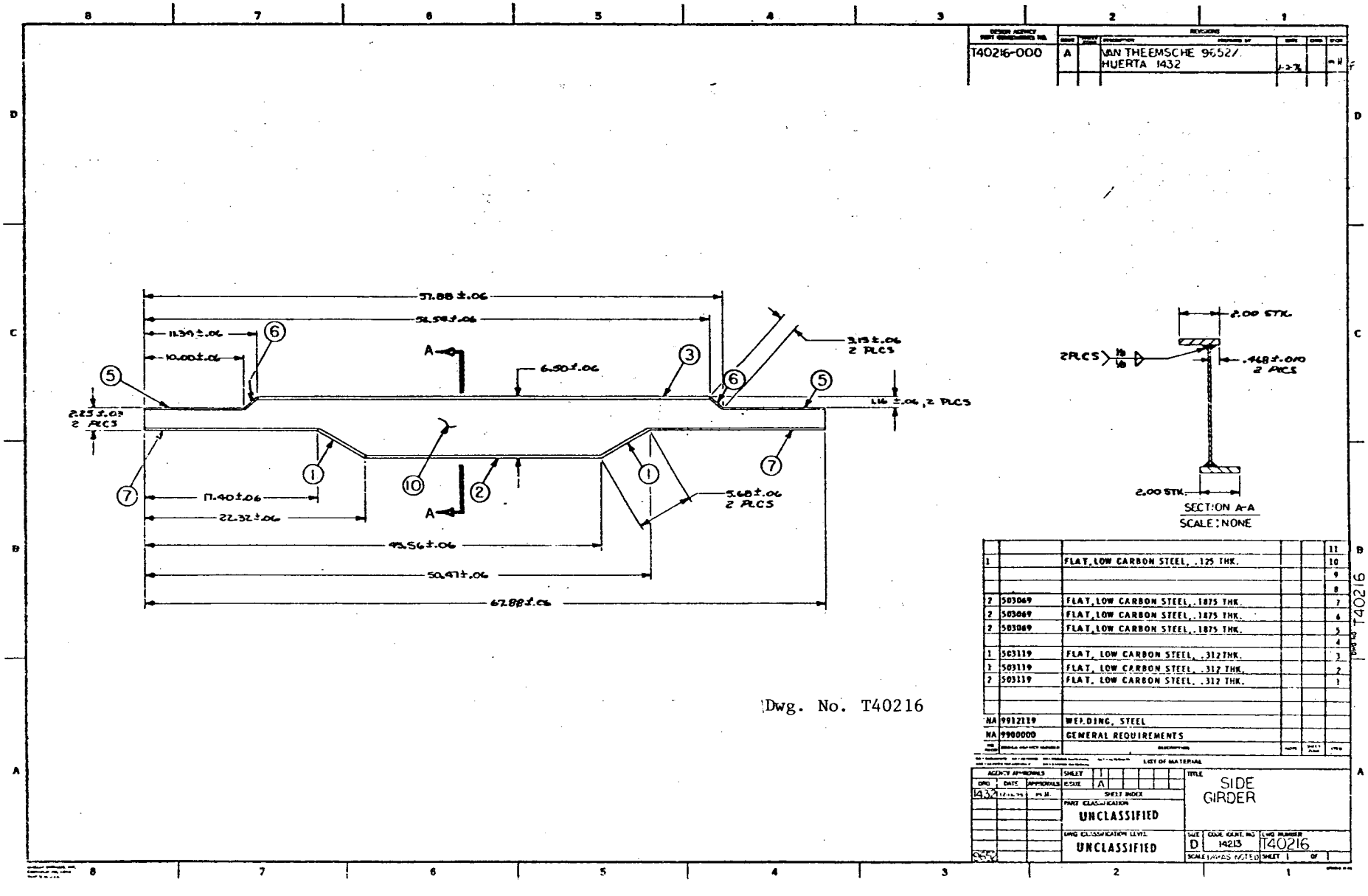

Figure B.1. Side Girder

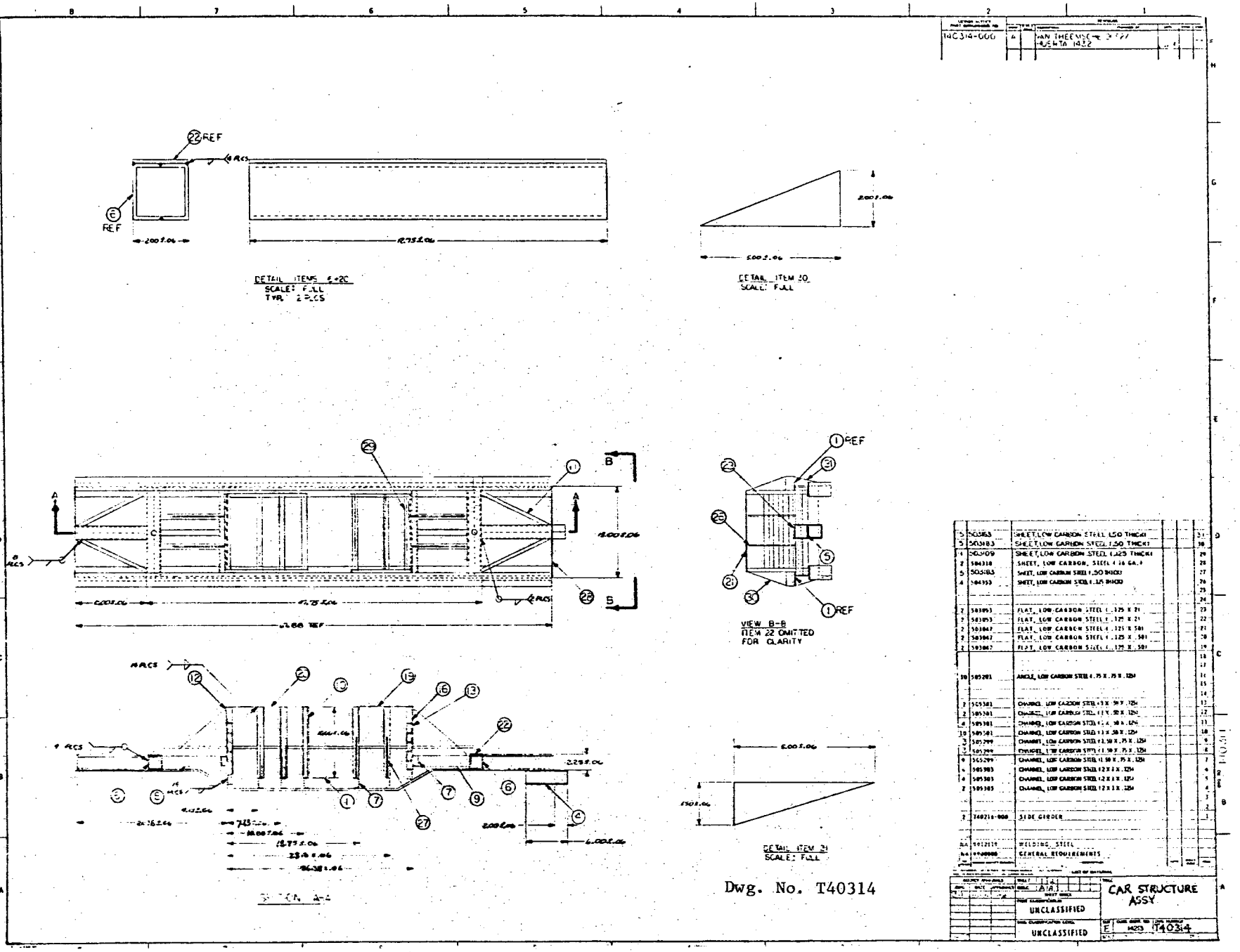

Figure B.2. Car Structure Assembly (Part I)

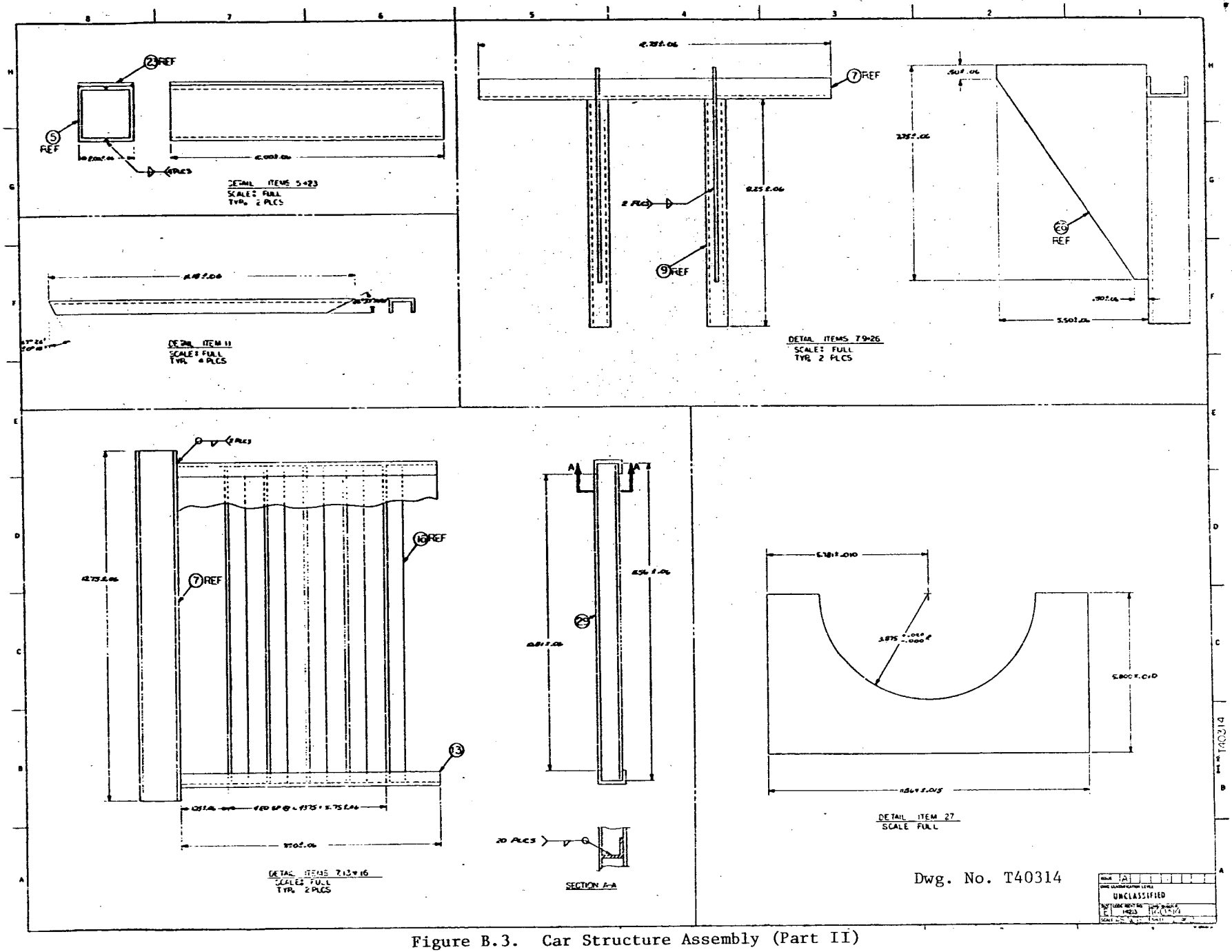

Figure B.3. Car Structure Assembly (Part II)

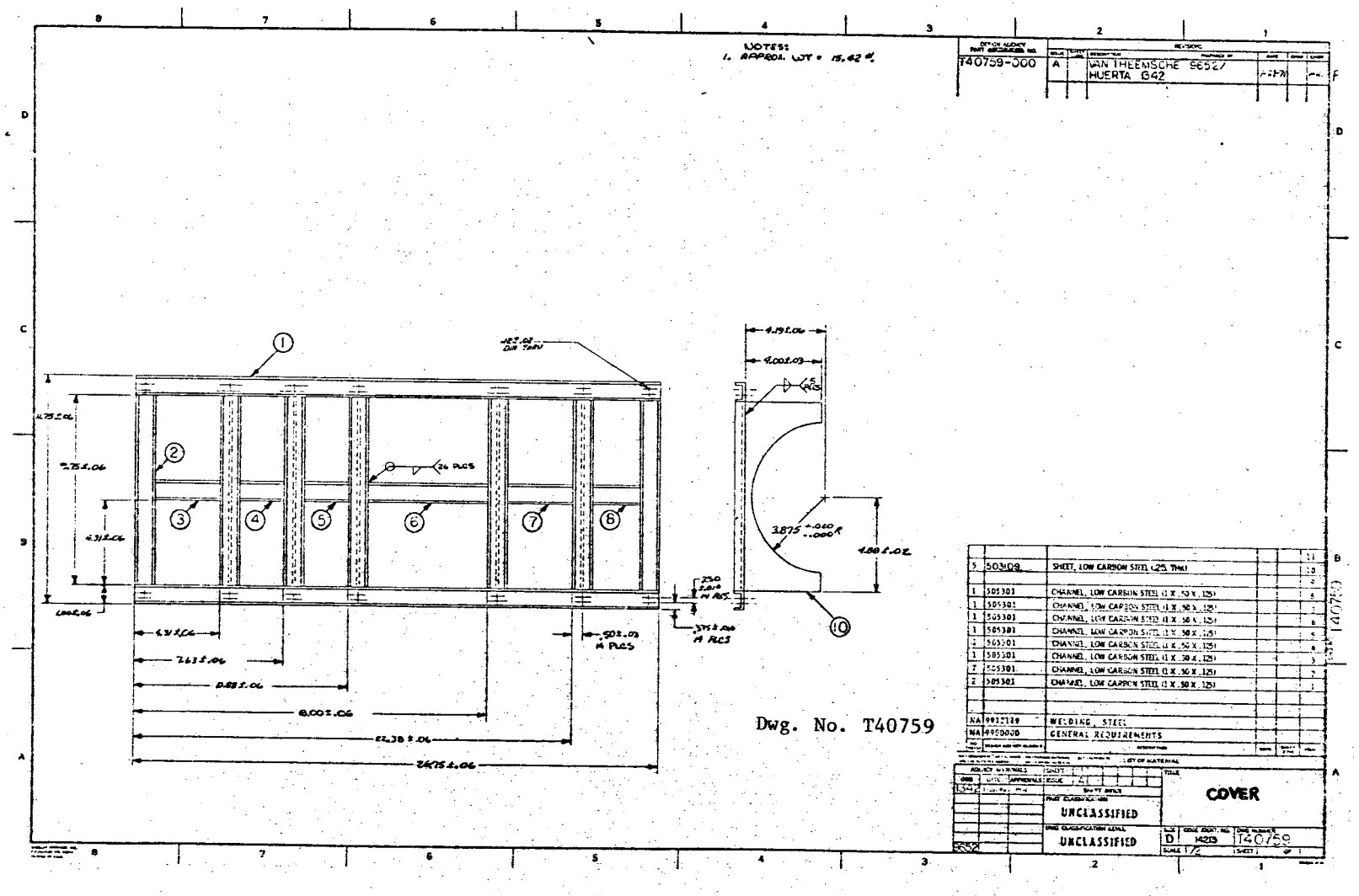

Figure B.4. Cover

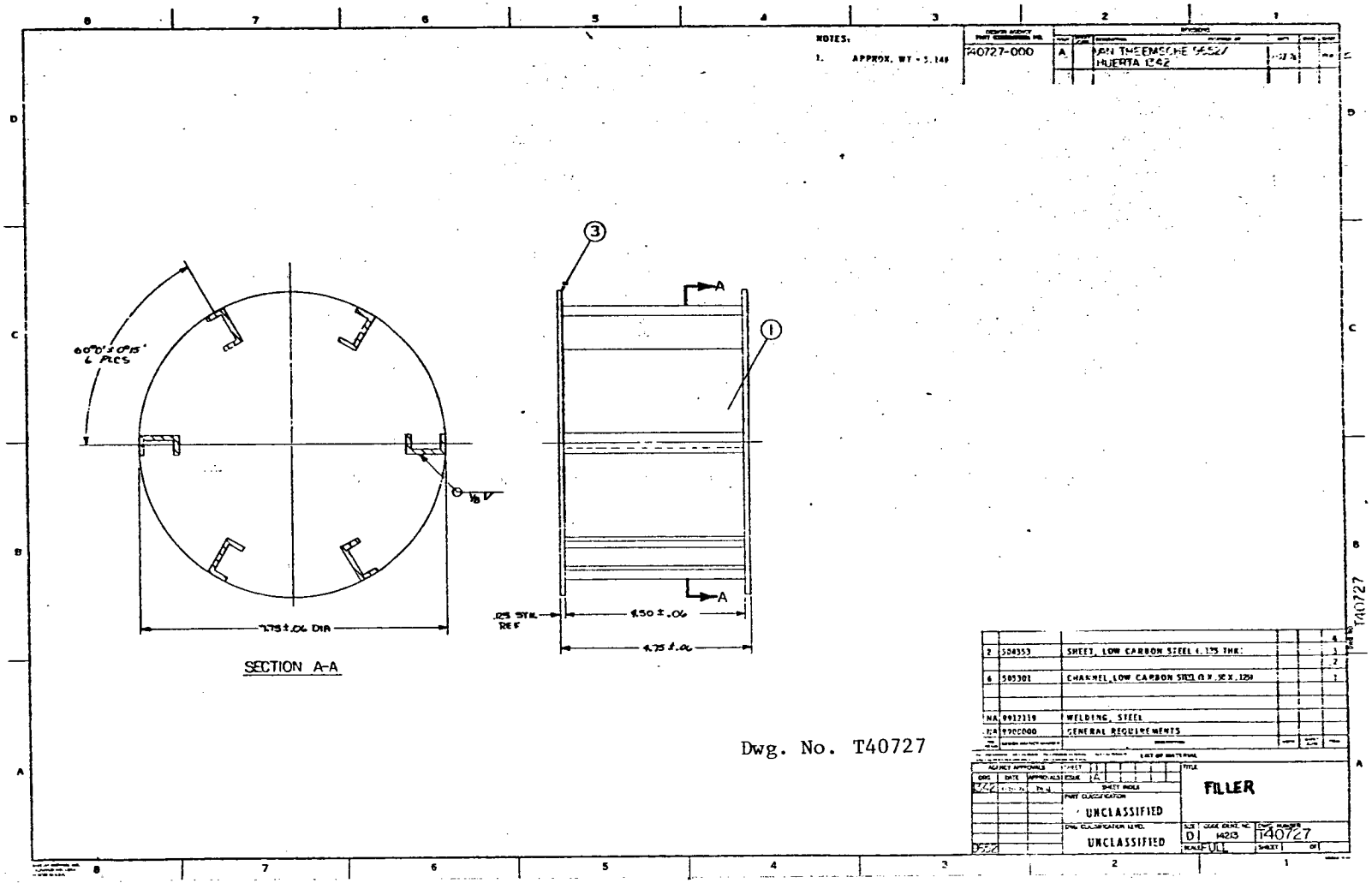

Dwg. No. T40727

Figure B.5. Filler

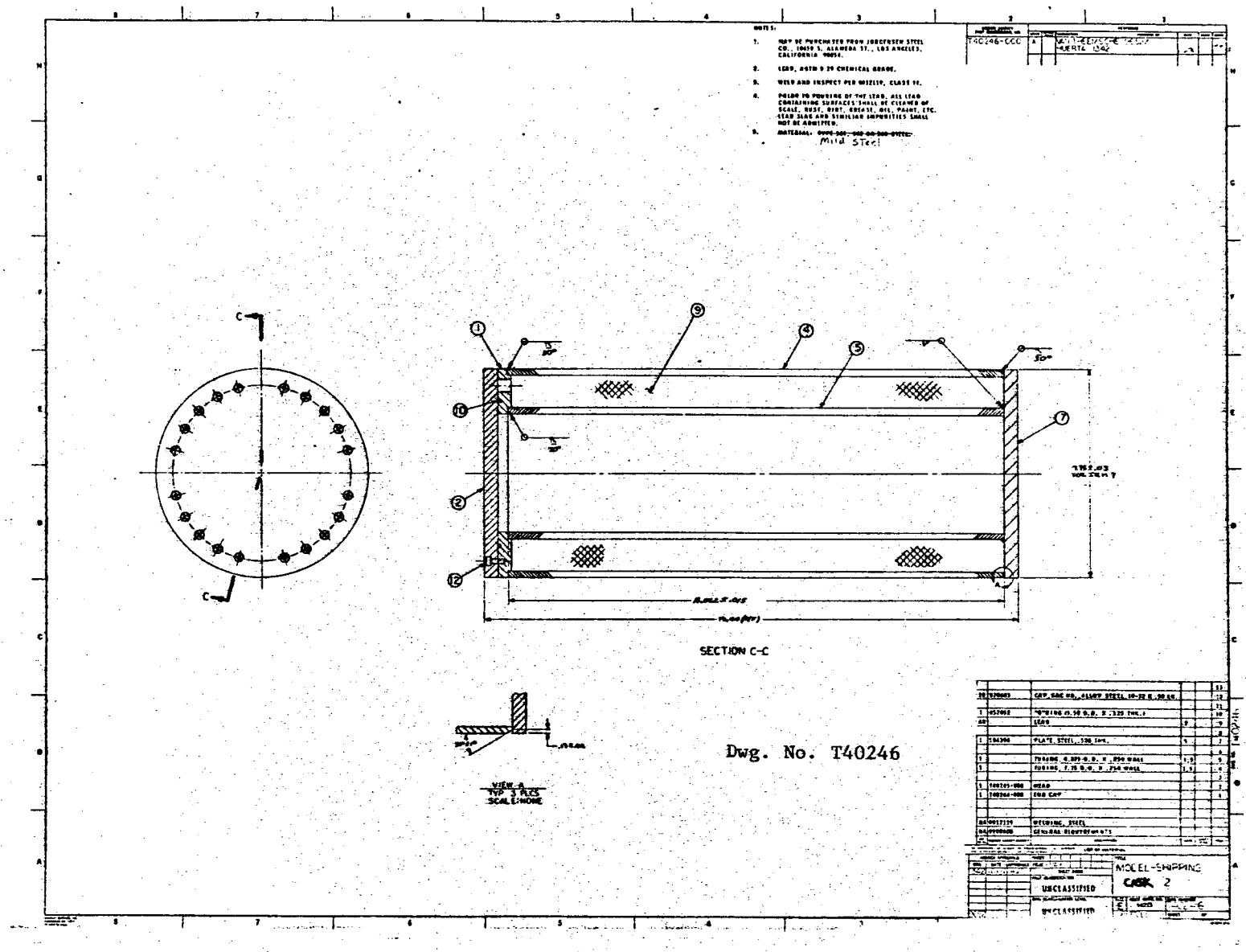

Figure B.6. Model Shipping Cask

APPENDIX C

Data From the Two Scale Model Tests

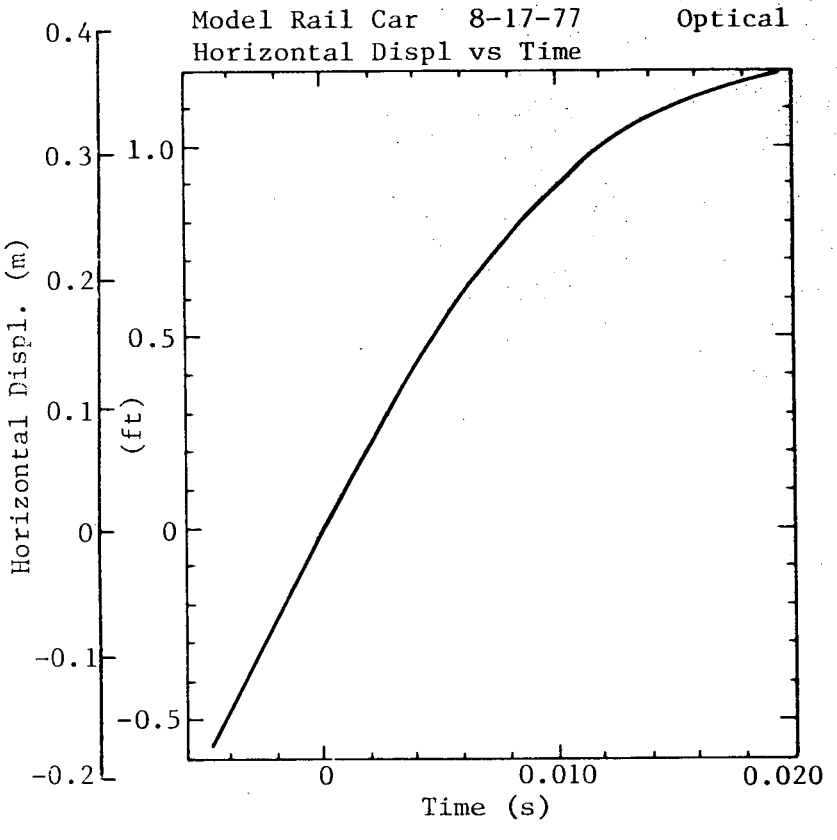

Figure C-1. Cask Horizontal Displacement vs Time From the First Model Test

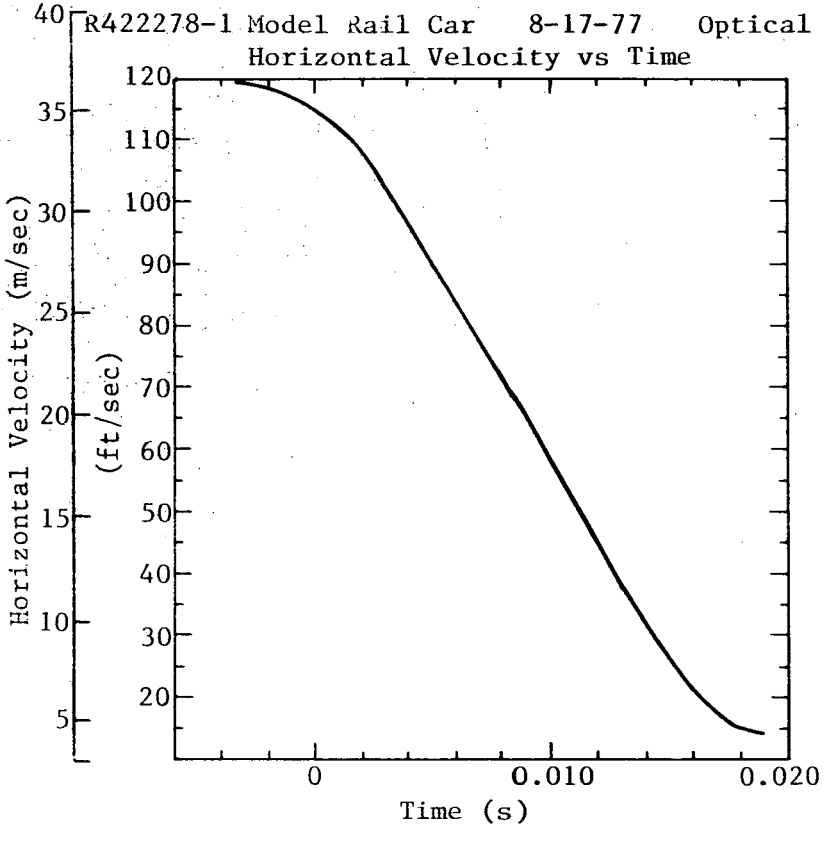

Figure C-2. Cask Horizontal Velocity vs Time From the First Model Test

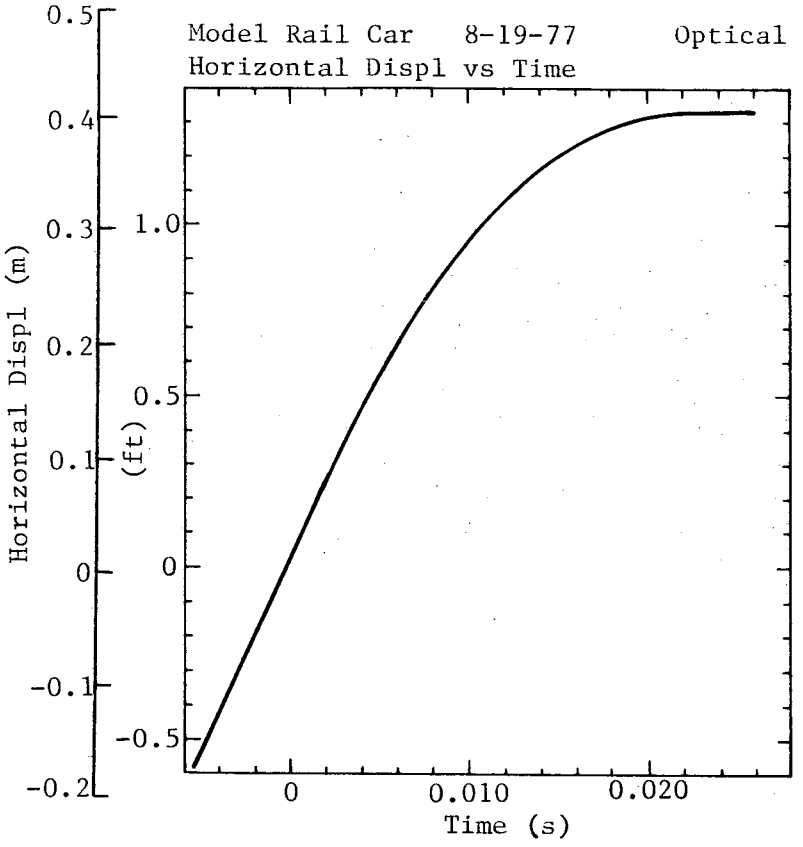

Figure C-3. Cask Horizontal Displacement vs Time From the Second Model Test

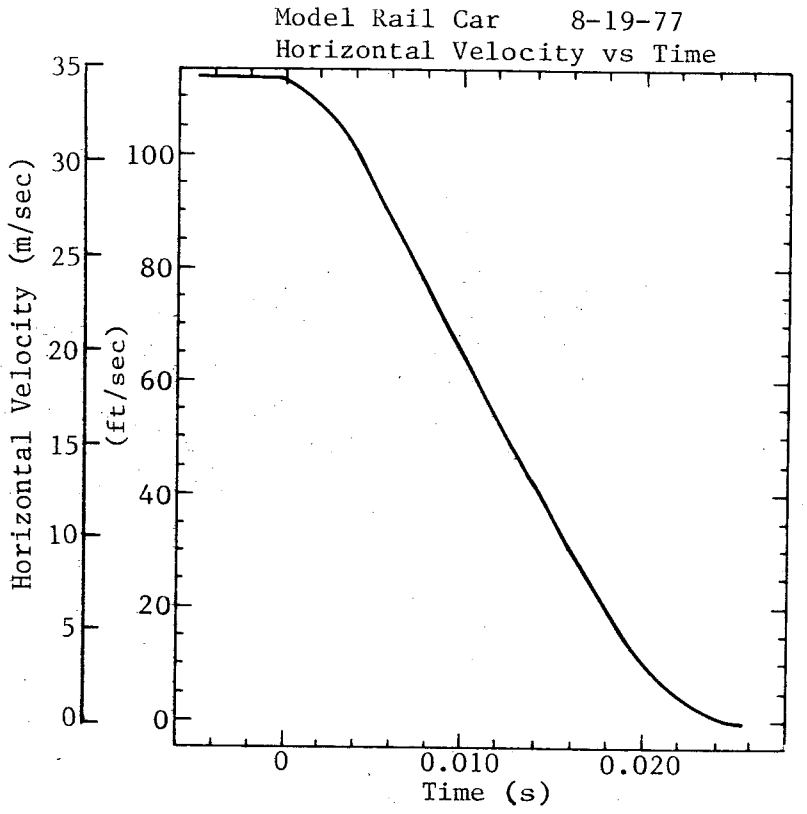

Figure C-4. Cask Horizontal Velocity vs Time From the Second Model Test

APPENDIX D

Data From the Full-Scale Test

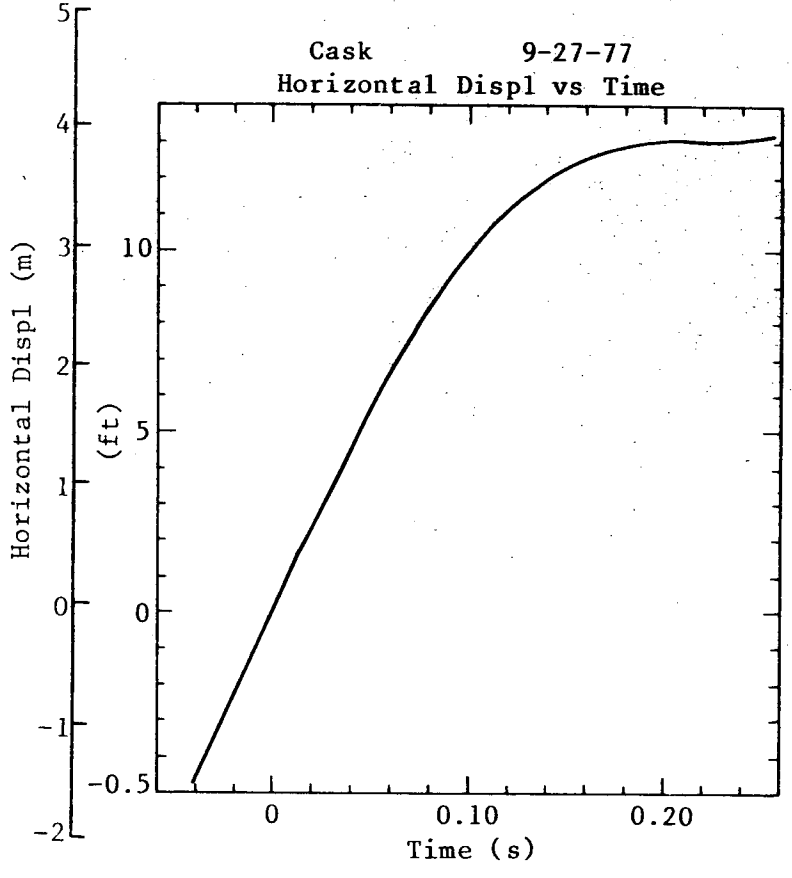

Figure D-1. Horizontal Cask Displacement vs Time (film data)

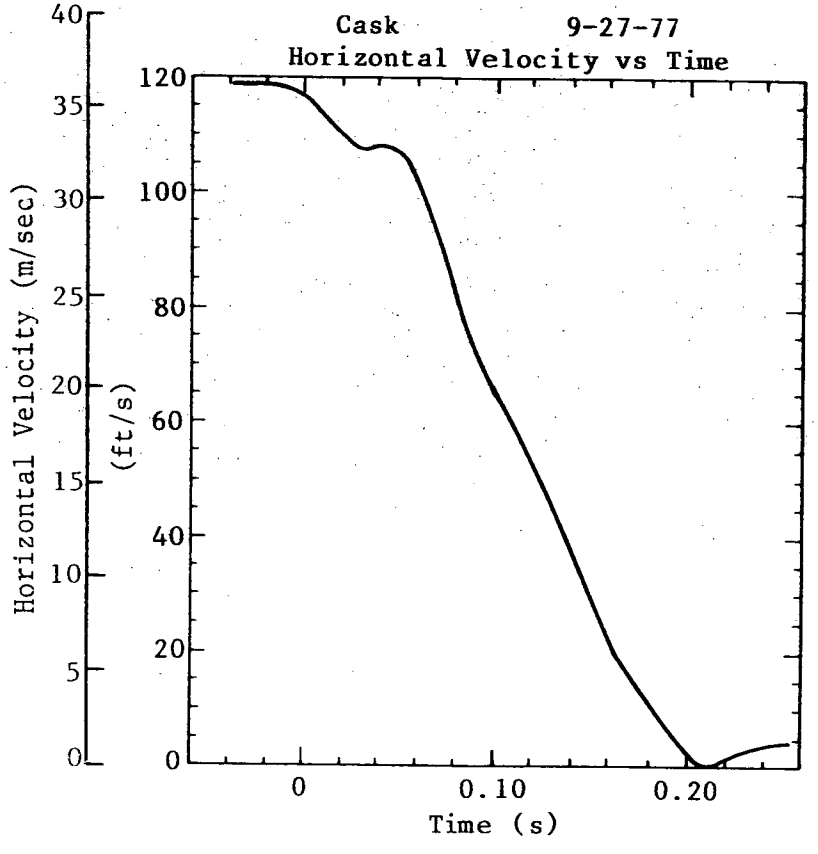

Figure D-2. Horizontal Cask Velocity vs Time (film data)

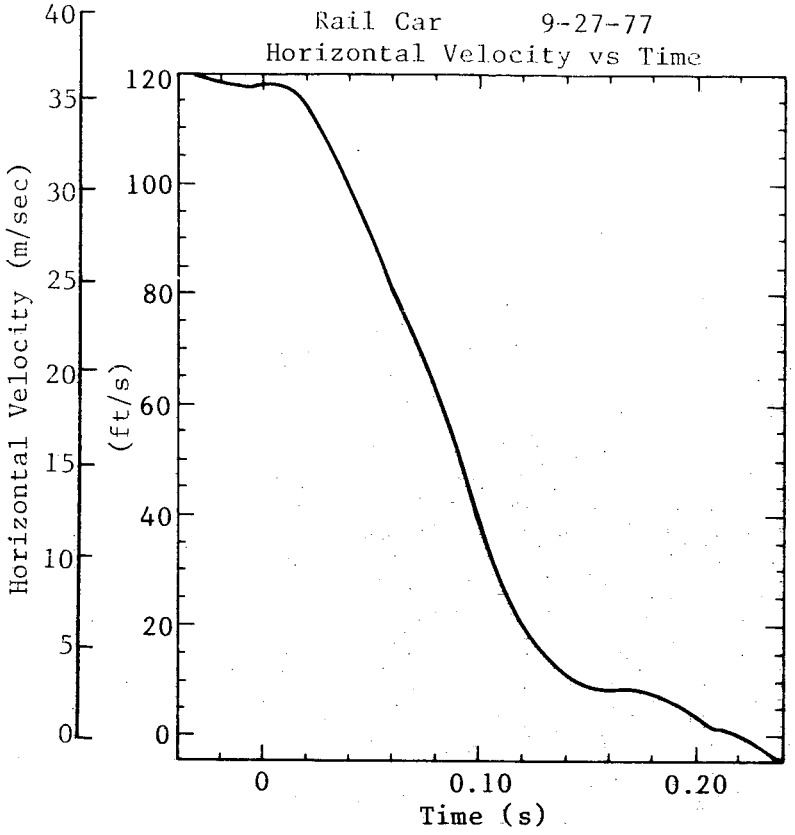

Figure D-3. Railcar Velocity vs Time. Data was obtained by following a point near the back end of the structure (film data)

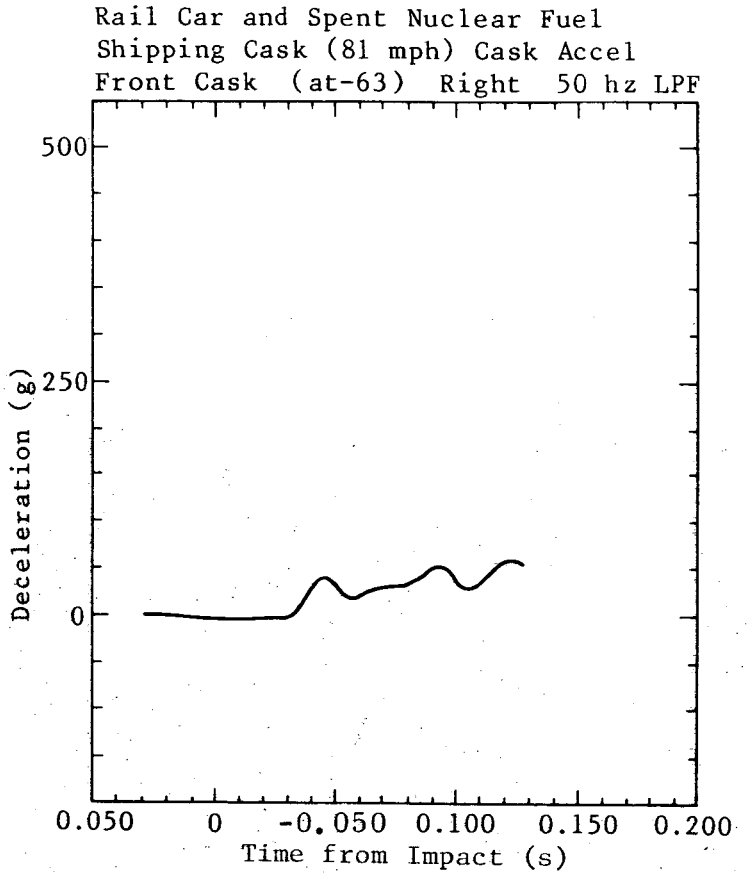

Figure D-4. Cask Deceleration vs Time (accelerometer data)

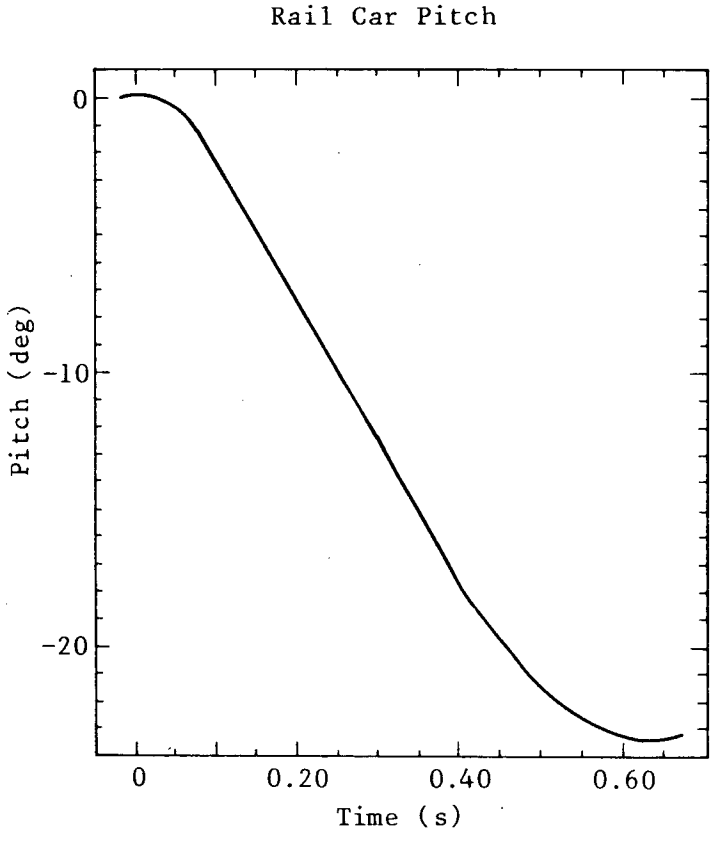

Figure D-5. Railcar Pitch vs Time (film data)

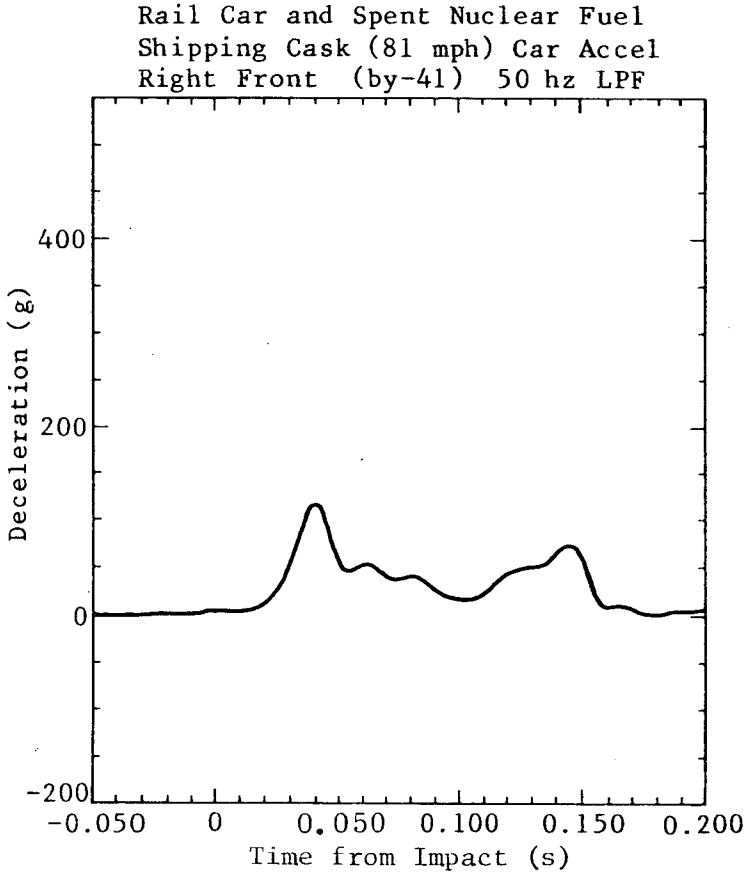

Figure D-6. Railcar Deceleration vs Time. Data was obtained from a point near the back end of the structure (accelerometer data)

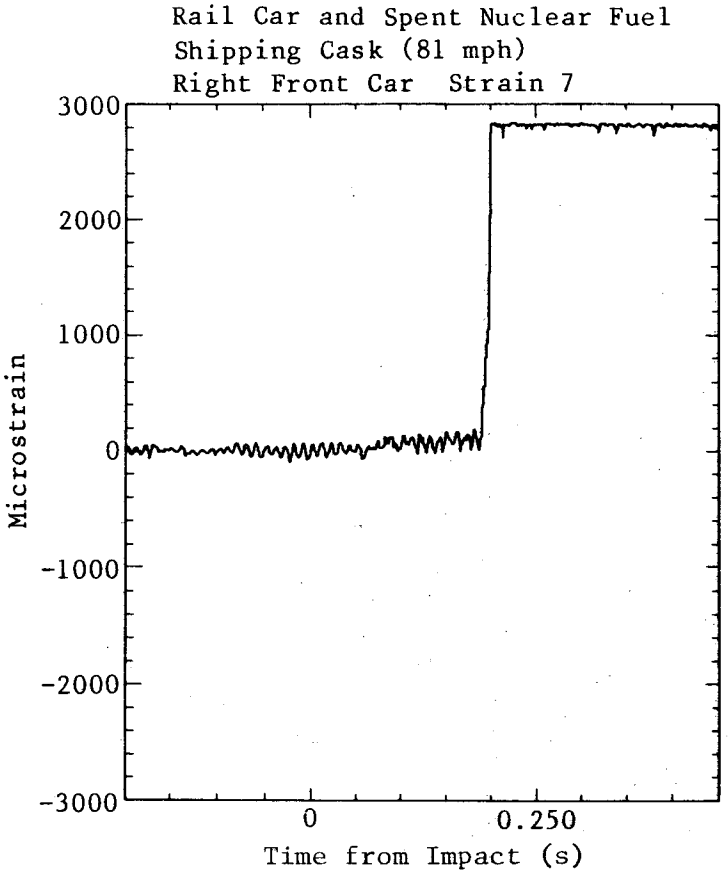

Figure D-7. Strain Reading From the Right Front Side of the Railcar Frame by Bolster

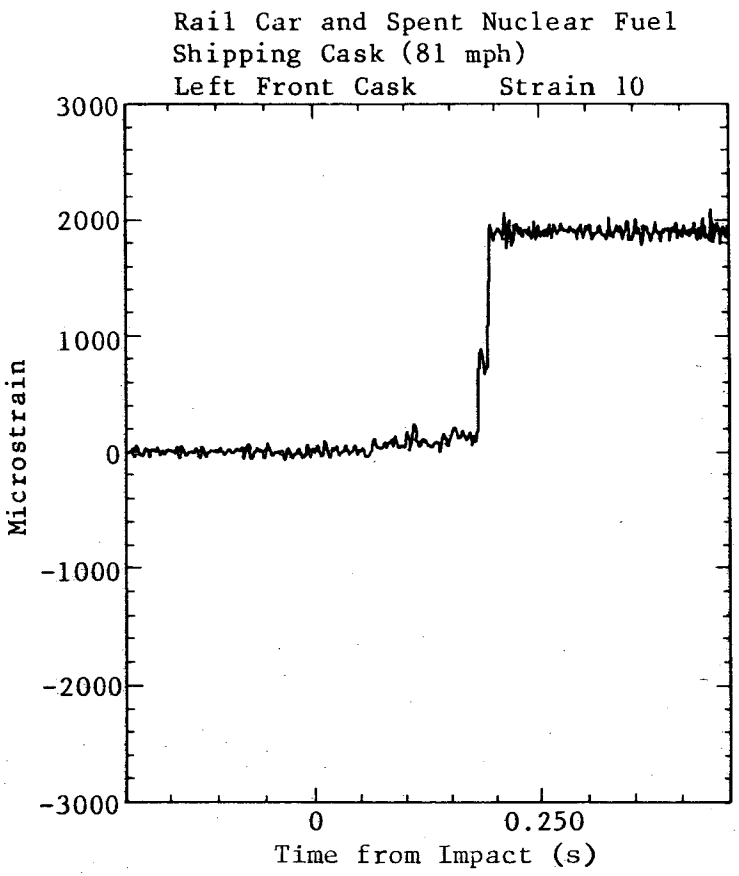

Figure D-8. Strain Reading From the Left Front Side of the Railcar Frame by Bolster

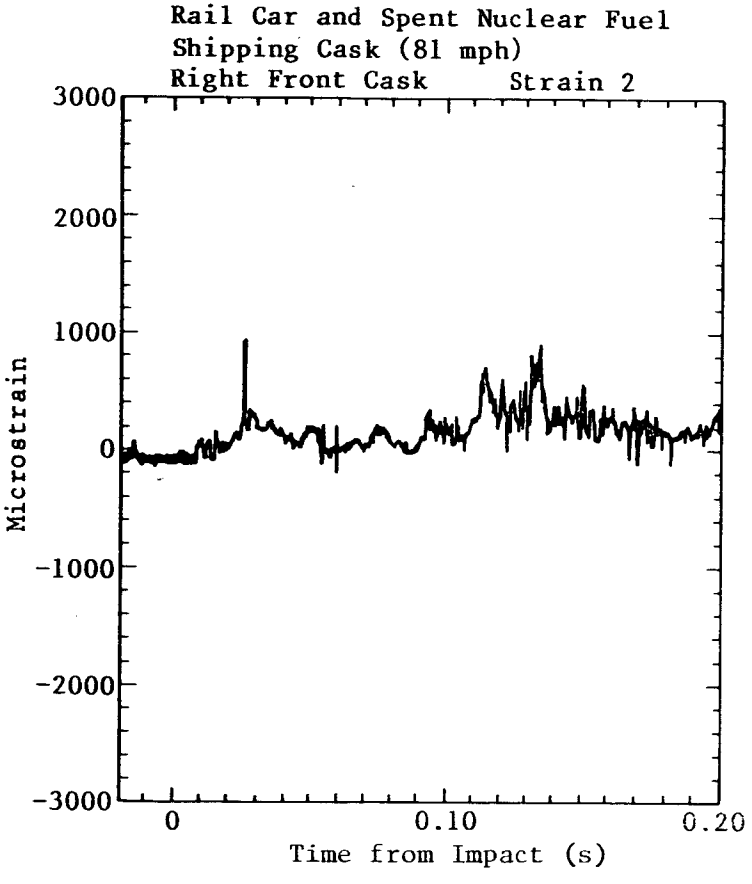

Figure D-9. Strain Reading From the Right Side of the Cask Head

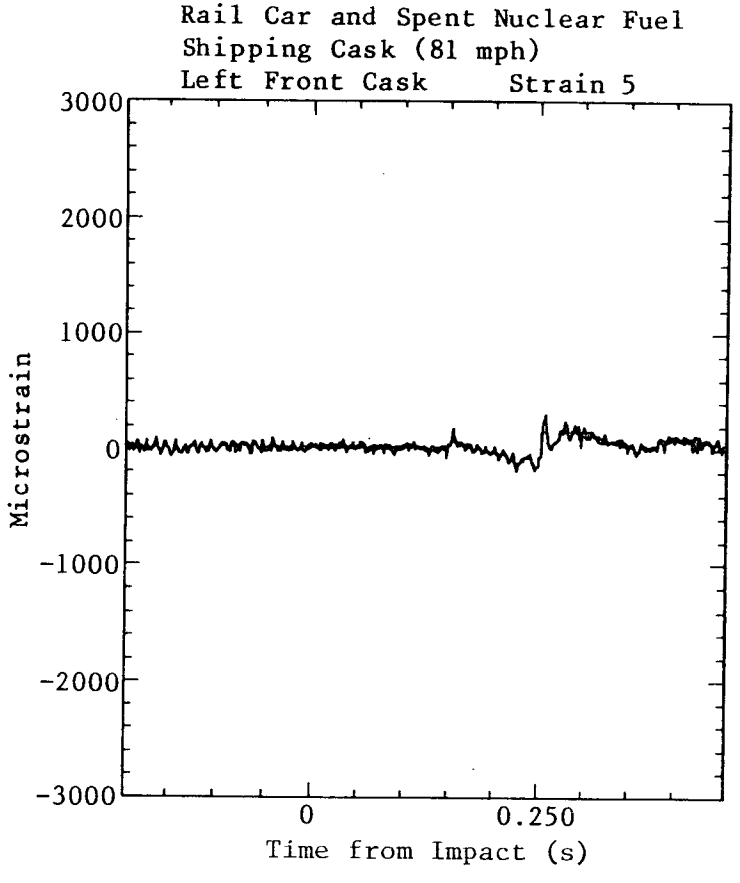

Figure D-10. Strain Reading From the Left Side of the Cask Head

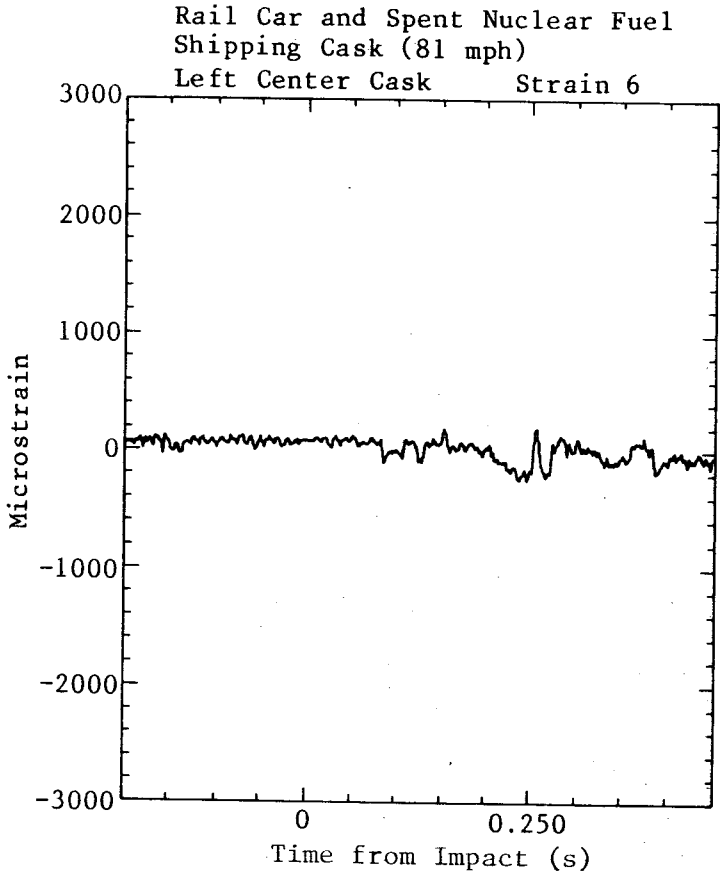

Figure D-11. Strain Reading From the Left Side of the Cask Body

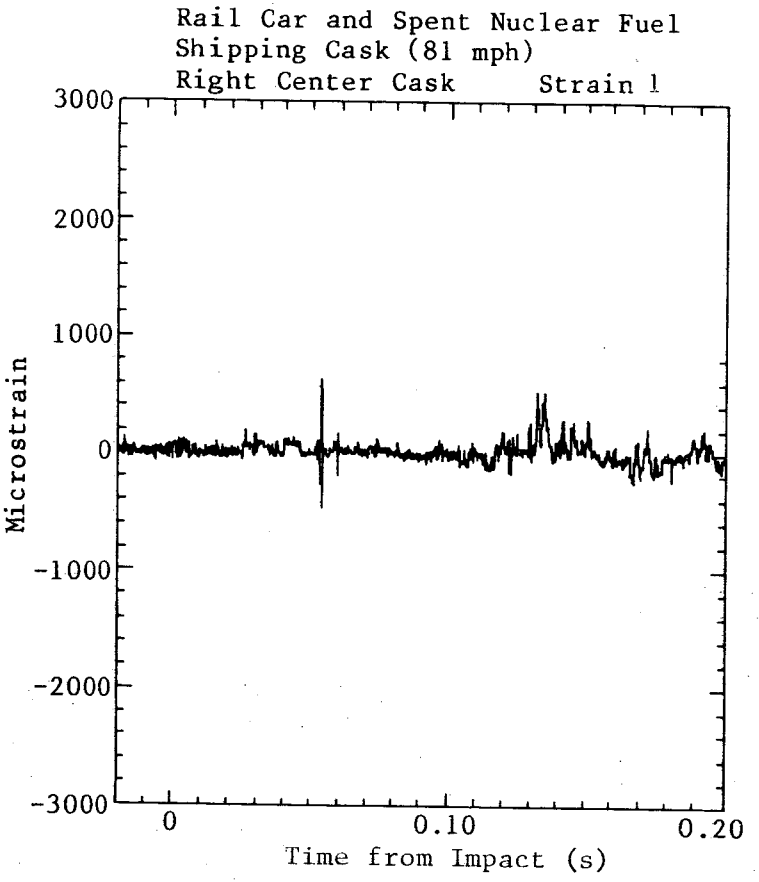

Figure D-12. Strain Reading From the Right Side of the Cask Body

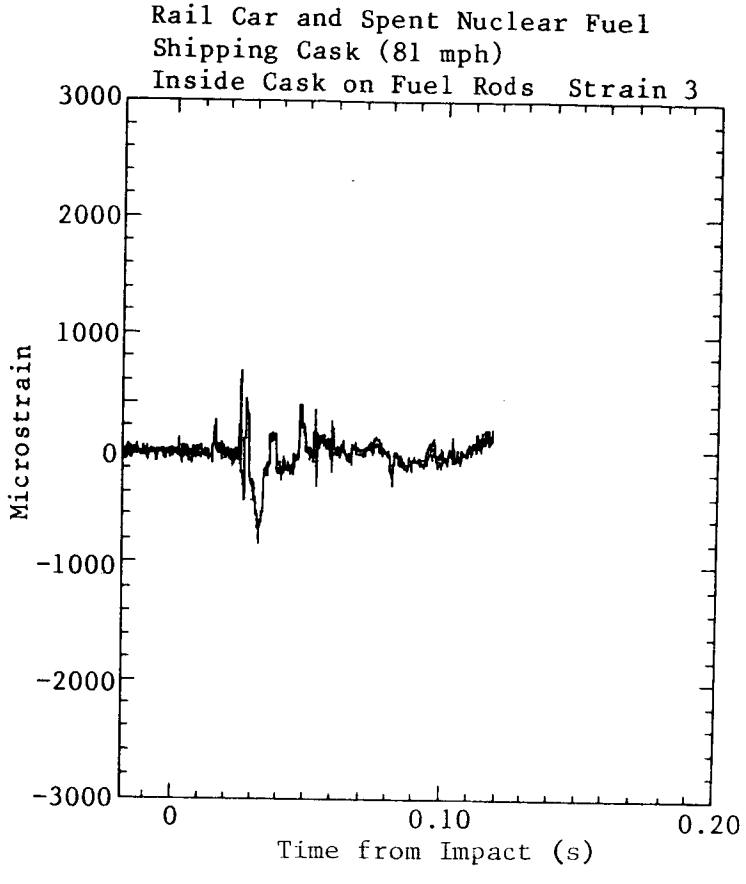

Figure D-13. Strain Reading From the First Instrumented Fuel Rod

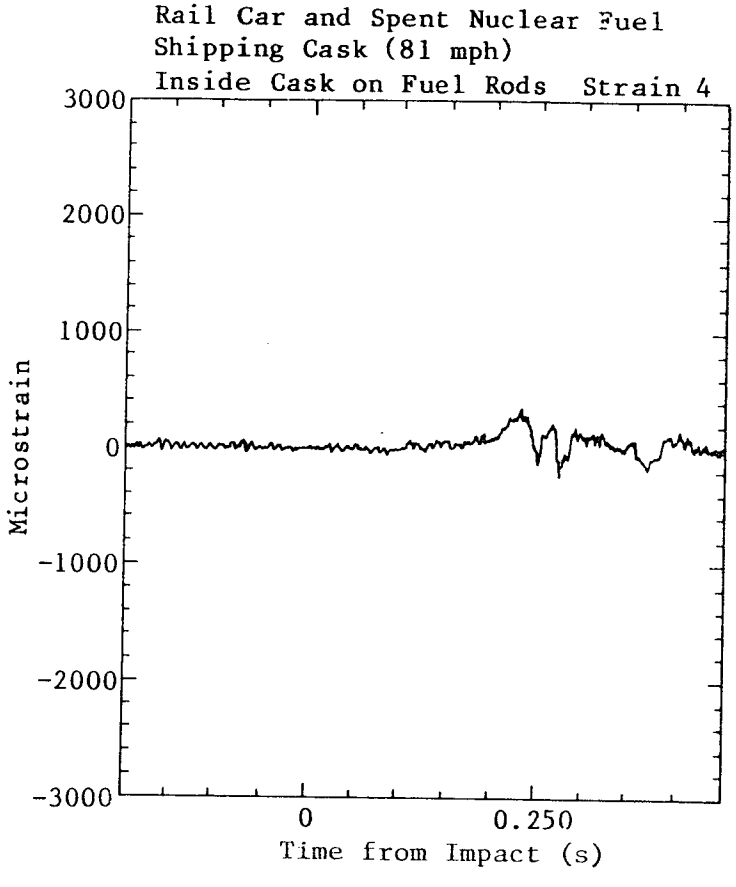

Figure D-14. Strain Reading From the Second Instrumented Fuel Rod

References

[1]H. R. Yoshimura and M. Huerta, Full-Scale Tests of Spent-Nuclear-Fuel Shipping Systems, SAND76-5707 (Albuquerque: Sandia Laboratories, July 1976). Also, IAEA-SR-10/17 (International Atomic Energy Administration, July 1976).

[2]M. Huerta, Analysis, Scale Modeling, and Full-Scale Tests of a Truck Spent-Nuclear-Fuel Shipping System in High Velocity Impacts Against a Rigid Barrier, SAND77-0270 (Albuquerque: Sandia Laboratories, April 1978).

[3]M. Huerta to H. R. Yoshimura, "Analysis of the OROX 300 Railcar and Cask Impact Test," (Albuquerque: Sandia Laboratories, September 20, 1977). Memorandum.

[4]V. K. Gabrielson and R. T. Reese, SHOCK Code Users Manual, A Computer Code to Solve the Dynamic Response of Lumped-Mass Systems, SCL-DR-69-98 (Livermore: Sandia Laboratories, November 1969).

DISTRIBUTION:
TIC-4500-R69 UC-71 (166)

US Department of Energy (2)
Albuquerque Operations Office
P.O. Box 5400
Albuquerque, NM 87185
Attn: K. Carlson
R. Y. Lowrey

Allied-General Nuclear Services
P.O. Box 847
Barnwell, SC 29812
Attn: P. F. Highberger

Applied Science and Technology
3344 North Torrey Pines Court
Suite 220
La Jolla, CA 92037

Atomics International
P.O. Box 309
Canoga Park, CA 91304
Attn: K. Foster

Battelle Memorial Institute
Office of Nuclear Waste Isolation
505 King Avenue
Columbus, OH 43201
Attn: R. W. Peterson, Proj. Mgr.

Battelle Memorial Institute
Pacific Northwest Laboratories
P.O. Box 999
Richland, WA 99352
Attn: K. Schneider

The Boeing Company
Nuclear Power Systems Equipment
P.O. Box 3707, M/S 9A-48
Seattle, WA 98124
Attn: S. M. Graves, Director

Chem-Nuclear Systems, Inc.
P.O. Box 1866
Bellevue, WA 98009
Attn: K. H. Kinkade

EG&G Idaho, Inc.
P.O. Box 1625
Idaho Falls, ID 83401
Attn: J. D. McKinney

E. I. du Pont de Nemours & Co
Savannah River Plant
Bldg 773-A
Aiken, SC 29801
Attn: F. D. King

Exxon Nuclear Company
777 106th Avenue NE, C-00777
Bellevue, WA 98055
Attn: J. H. Nordahl

Exxon Nuclear Company (2)
Research and Technology Center
2955 George Washington Way
Richland, WA 99352
Attn: E. E. Garrett
J. H. Riddle

General Atomic Company
P.O. Box 81608
San Diego, CA 92138
Attn: R. Burgoyne

General Electric Corporation
175 Curtner Avenue
San Jose, CA 95125
Attn: C. Davis

Hittman Nuclear and Development Corp
9190 Red Branch Road
Columbia, MD 21045
Attn: P. E. Blanchard

Lanson Industries, Inc.
P.O. Drawer 1107
Cullman, AL 35055
Attn: R. C. Humphrey

Monsanto Research Corporation
Mound Laboratory
P.O. Box 32
Miamisburg, OH 45342
Attn: R. K. Blauvelt

NL Industries, Inc.
P.O. Box 2046
Wilmington, DE 19899
Attn: D. G. Maxwell, Gen Mgr

DISTRIBUTION: (cont)

Nuclear Assurance Corporation
24 Executive Park West
Atlanta, GA 30329
Attn: C. Thorup, V Pres

Nuclear Packaging, Inc.
815 South 28th Street
Tacoma, WA 98409
Attn: J. D. Simchuk

Oak Ridge National Laboratory
P.O. Box X
Oak Ridge, TN 37830
Attn: L. B. Shappert

Oak Ridge National Laboratory
Building 9204-1
P. O. Box Y
Oak Ridge, TN 37830
Attn: J. G. Merkle

Ridihalgh, Eggers & Associates
2112 Iuka Avenue
Columbus, OH 43201
Attn: J. L. Ridihalgh

Science Applications, Inc.
Licensing & Risk Analysis Division
P.O. Box 843
Oak Ridge, TN 37830
Attn: W. R. Rhyne, Manager

Stanford Research Institute
Engineering Mechanics Group
Poulter Laboratory
333 Ravenwood
Menlo Park, CA 94025
Attn: J. D. Colton, Asst Mgr

Stearns-Roger Manufacturing, Inc.
P.O. Box 5888
Denver, CO 80217
Attn: W. H. Brinkman, V Pres

Teledyne Energy Systems
110 West Timonium Road
Timonium, MD 21093
Attn: W. C. Kincaide

Transnuclear, Inc.
One North Broadway
White Plains, NY 10601
Attn: L. Macklin

The Transport Environment
SR 285 Old Squaw Drive
Kitty Hawk, NC 27949
Attn: W. A. Brobst

US Department of Energy
Savannah River Operations Office
Spent Fuel Project Office
P.O. Box A
Aiken, SC 29801
Attn: R. P. Whitfield, Deputy Dir.

US Department of Transportation
Office of Hazardous Materials Operations
Material Transportation Bureau/RSPA
2100 2nd Street, SW
Washington, DC 20590
Attn: R. R. Rawl

US Nuclear Regulatory Commission (4)
Office of Standards Development
Mail Stop NL 5650
Washington, DC 20555
Attn: D. R. Hopkins, MS NL5650
W. H. Lahs, Jr., MS 1130SS
C. E. McDonald, MS 396-SS
J. C. Malaro, MS NL5650

Westinghouse Electric Corporation
P.O. Box W
Oak Ridge, TN 37830
Attn: J. E. Rutenber

Westinghouse Electric Corporation (3)
Hanford Engineering Development
Laboratory
P.O. Box 1970
Richland, WA 99352
Attn: D. M. Bosi
E. T. Weber
S. R. Fields

T. A. Duffey
P.O. Box 4404, Station A
Albuquerque, NM 87106

K. Gablin
6749 Towne Lane Road
McLean, VA 22101

R. H. Jones
P.O. Box 24036
San Jose, CA 95154

DISTRIBUTION: (cont)

US Department of Energy (6)
Energy Technology - Waste
Washington, DC 20545
Attn: O. P. Gormley
T. Anderson
S. Meyers
F. P. Falci
J. A. Sisler
M. J. Lawrence

Los Alamos Scientific Laboratory
P.O. Box 1663
Los Alamos, NM 87545
Attn: D. Smith

M. Huerta (10)
3616 Derick
El Paso, TX 79924

1500 W. A. Gardner
1530 W. E. Caldes
1535 D. C. Bickel
4400 A. W. Snyder
4410 D. J. McCloskey
4440 G. R. Otey
4442 W. A. Von Riesemann
4500 E. H. Beckner
4550 R. M. Jefferson
4550 TTC Master File
4551 R. E. Luna
4551 R. P. Sandoval
4551 J. D. McClure
4551 TTC Library (5)
File Ref: 3003.000
4552 R. B. Pope
4553 H. R. Yoshimura (10)
4553 D. R. Stenberg
4700 J. H. Scott
5500 O. E. Jones
5520 T. B. Lane
5522 T. G. Priddy
5523 R. C. Reuter
5524 R. D. Krieg
5531 S. W. Key
8120 W. E. Alzheimer
8214 M. A. Pound
3141 L. J. Erickson (5)
3151 W. L. Garner (3)
For DOE/TIC (Unlimited Release)